工學碩士 學位論文

# A Study on Improved Algorithm for MIMO Antenna Measurement

指導教授 閔 庚 植

**2007** 年 **2** 月

韓國海洋大學校 大學院

電 波 工 學 科

**Tran Thanh Ngon**

本 論文을 Tran Thanh Ngon의 工學碩士
學位論文으로 認准함.

委 員 長 : 工學博士 河 潤 秀 (印)

委 員 : 工學博士 朴 世 鉉 (印)

委 員 : 工學博士 閔 庚 植 (印)

2007年 2月

韓國海洋大學校 大學院

電 波 工 學 科

Tran Thanh Ngon

# Abstract

This thesis presents the improvement of algorithm for antenna measurement software and development of measurement testbed for multi-input multi-output (MIMO) antenna measurement. Firstly, the algorithm for antenna measurement software is improved to operate with variety types of equipments and reduce measurement noise. After that, this software is used to measure 3 parameters of MIMO antennas. Finally, to measure other parameters of MIMO antennas and MIMO systems, the MIMO testbed is developed and presented. As the results, the improved software can be used to measure gain, 2D & 3D radiation pattern, for single antenna, and polarization, pattern diversity, polarization diversity and pattern correlation, for MIMO antenna. The measurement results are very beautiful when the noise filter algorithm is applied. In MIMO testbed design, direct conversion technique is used for analog front end circuit design. Front end circuits are also coupled with baseband DSP algorithm. The result is that front end circuits have compact size and wide bandwidth. Finally, hardware and software configurations of MIMO testbed are designed and presented.

# Acknowledgments

I am grateful to many people who supported, helped and encouraged me during two year of my study in Korea:

First of all, my advisor, Professor Kyeong-Sik Min, who fully supported for my study and living at Korea Maritime University and gave me good advises for my research work. I also thank to committee members, Professor Yun-Su Ha and Doctor Se-Hyun Park, for their comments and review of my thesis.

My friends, Korean and Vietnamese friends, who helped and understood me as well as shared my thought.

Finally, my parents, sisters and brothers, who continuously encouraged me during the time I stay in Korea.

# CONTENTS

List of figures ..... 3

List of tables ..... 6

**Chapter 1:** Introduction. ..... 7

**Chapter 2:** Algorithm of antenna measurement software with noise reduction. ..... 9

2.1 Objective. ..... 9

2.2 Improvement of software structure. ..... 9

2.2.1 Measurement configuration and new software structure. ..... 9

2.2.2. Measurement results. ..... 12

2.3 Filter algorithm for noise reduction. ..... 17

2.3.1. Filter algorithm. ..... 18

2.3.2. Experimental results of filter algorithm. ..... 22

2.4 Summary. ..... 27

**Chapter 3:** Measurement of key parameters of MIMO antenna. ..... 28

3.1. Objective. ..... 28

3.2. Measurement configuration. ..... 29

3.2.1 Pattern diversity, polarization diversity and calculation of pattern correlation. ..... 29

3.2.2. Measurement of mutual coupling. ..... 30

3.3. Results and discussions. ..... 30

3.3.1 Pattern diversity and polarization diversity ..... 30

3.3.2. Pattern correlation. ..... 33

3.3.3. Mutual coupling. ..... 33

3.4. Summary. ..... 34

**Chapter 4:** Design of multi-band MIMO test-bed ..... 35

4.1. Objective. ..... 35

4.2. Design of analog RX circuit. ..... 37

4.2.1. Receiver Architecture and Signal Analysis. ..... 37

4.2.2. Simulation and Measurement Results. ..... 40

4.3. Design of analog TX circuit ..... 46

4.3.1. Transmitter architecture and signal analysis. ..... 47

4.3.2. Fabrication and Measurement Results. ..... 48

4.4. Design of 2x2 MIMO measurement system. ..... 52

4.4.1 Hardware configuration. ..... 52

4.4.2 Software configuration. ..... 52

4.5. Summary. ..... 54

**Chapter 5:** Conclusion. ..... 56

**References** ..... 57

# LIST OF FIGURES

Fig. 2.1 Configuration of antenna measurement ..... 10

Fig. 2.2 Structure of measurement software ..... 11

Fig. 2.3 Common flow chart of measurement program ..... 12

Fig. 2.4 Antenna measurement in anechoic chamber ..... 13

Fig. 2.5 Radiation pattern of helical antenna ..... 13

Fig. 2.6 Gain of helical antenna ..... 14

Fig. 2.7 Two components of E-field of helical antenna ..... 15

Fig. 2.8 Axial ratio of helical antenna ..... 16

Fig. 2.9 Integrated antenna measurement software ..... 16

Fig. 2.10 Original signal of radiation pattern ..... 17

Fig. 2.11 Illustration of $D''$[i] and $SL$ ..... 21

Fig. 2.12 Reference signal ..... 24

Fig. 2.13 Signal filtered by TM filter $N = 5$ & 150 ..... 24

Fig. 2.14 Signal filtered by SM filter $W = 5$ & 9 ..... 25

Fig. 2.15 Signal filtered by TAM filter ..... 25

Fig. 2.16 Signal filtered by SAM filter ..... 26

Fig. 2.17 Signal filtered by SAM and TAM ..... 26

Fig. 3.2 Sample of EUT (PDA size 75×110×7 mm) ..... 29

Fig. 3.3 Radiation pattern of element #1 ..... 31

Fig. 3.4 Radiation pattern of element #2 ..... 32

Fig. 3.5 Radiation pattern of element #3 ..... 32

Fig. 3.6 Radiation pattern of element #4 ..... 32

Fig. 3.7 The coupling coefficient between antenna elements..... 34

Fig. 4.1 A block diagram of MIMO testbed ..... 35

Fig. 4.2 Receiver architecture and signals in direct down-conversion receiver ..... 38

Fig. 4.3 Implementation of algorithm in DSP unit ..... 39

Fig. 4.4 ADS model of analog front-end circuit..... 40

Fig. 4.5 Fabrication of the circuit ..... 41

Fig. 4.6 Amplitude ratio at port 2 and 3 of phase shifter..... 42

Fig. 4.7 Phase difference between port 2 and 3 of phase shifter ..... 42

Fig. 4.8 Return loss at 3 ports of phase shifter ..... 43

Fig. 4.9 Amplitude imbalance coefficient of quadrature down converter..... 44

Fig. 4.10 Phase imbalance coefficient of quadrature down converter..... 44

Fig. 4.11 Lissajuos graph of the I and Q signal at 1.8 GHz..... 45

Fig. 4.12 Lissajuos graph of the I and Q signal at 4.0 GHz..... 45

Fig. 4.13 Lissajuos graph of the I and Q signal at 5.6 GHz..... 46

Fig. 4.14 Transmitter architecture and signals in direct up-conversion transmitter ..... 47

Fig. 4.15 Spectrum of signal at the output of quadrature up-converter ..... 48

Fig. 4.16 Fabrication of the circuit ..... 49

Fig. 4.17 Measurement setup..... 49

Fig. 4.18 Amplitude imbalance coefficient of quadrature up converter..... 50

Fig. 4.19 Phase imbalance coefficient of quadrature up converter..... 50

Fig. 4.20 Spectrum of output signal before compensation ..... 51

Fig. 4.21 Spectrum of output signal after compensation ..... 51

Fig. 4.22 AD, DA system from Brains Corporation..... 53

Fig. 4.23 Configuration of MIMO testbed ..... 53

Fig. 4.24 Software components ..... 54

Fig. 4.25 Software for I/Q imbalance compensation ..... 54

# LIST OF TABLES

Table 3.1 Pattern correlation of antenna elements on measurement planes ..... 33

Table 4.1 Specifications ..... 36

# CHAPTER 1

# INTRODUCTION

The objectives of this thesis are to improve algorithm for antenna measurement software and develop measurement testbed for multi-input multi-output (MIMO) antenna measurement. The study is divided in 3 steps. Firstly, the algorithm for antenna measurement software is improved to operate with variety types of equipments and reduce measurement noise. After that, this software is used to measure 3 parameters of MIMO antennas. Finally, to measure other parameters of MIMO antennas and MIMO systems, the MIMO testbed is developed and presented.

The original antenna measurement software in anechoic chamber at Korea Maritime University is presented in [1]. This software has some limits, such as: be only operated on CONECT GPIB interface card, can be used to measure two parameters of antenna, antenna gain and radiation pattern, and in some cases, measurement results are noisy. Therefore, the algorithm of software in [1] is improved so that it can be operated on variety types of equipments, can be modified easily and can be used to measure 4 parameters with noise reduction function. Four parameters are antenna gain, radiation pattern, polarization and 3-D radiation pattern.

With the development of wireless communication systems, MIMO antennas are developed. It is necessary to measure parameters of MIMO antenna for evaluating antenna performance. The improved antenna measurement software can be used to measure 3 parameters of MIMO antennas. These parameters are pattern diversity, polarization diversity and pattern correlation.

The above parameters of MIMO antennas are measured independently of MIMO systems that include the effect of transmission channel, antennas, circuits and signal processing algorithm. To evaluate other parameters of MIMO antennas on MIMO system such as antenna type, spacing, configuration, number of elements [2]… the MIMO testbed is needed. In addition, in MIMO research, theory and simulations typically show the

corresponding gains under ideal conditions, hardware platforms and testbeds are essential in validating these gains in real channels and in the presence of implementation impairments [3]. As shown in [3], the MIMO testbed is also useful in education at universities.

To develop the improved algorithm for antenna measurement software, the Visual Basic and C++ Builder programming languages are used. The improved algorithm is evaluated by theoretical analysis and experimental measurement results in anechoic chamber.

To develop a MIMO testbed, Agilent Advance Design System (ADS) software is used to simulate the RF analog circuits, AD/DA systems from Brains Corporation and personal computer (PC) are used as the baseband DSP hardware of testbed. These circuits are fabricated and its parameters are measured and presented; some DSP functions are developed and shown in this thesis. As shown in [3], the development of MIMO testbed require long time because it relates to many study fields such as coding, synchronization, the operation and optimal programming of baseband processors, the impact of radio frequency (RF) imperfections on signals, the operation of test equipment, and deployment in realistic test scenarios. Therefore, in this thesis, the testbed design is not complete; some works remains for further study.

In this thesis, chapter 1 is the introduction, chapter 2 presents algorithm of antenna measurement software with noise reduction, chapter 3 presents the measurement of key parameters for MIMO antenna, chapter 4 presents the design of multi-band MIMO testbed and chapter 5 is the conclusions.

# CHAPTER 2

# ALGORITHM OF ANTENNA MEASUREMENT SOFTWARE WITH NOISE REDUCTION

## 2.1. Objective

This chapter presents the algorithm improvements of the antenna measurement software shown in [1]. The software in [1] has some limits such as: be only operated on CONECT GPIB interface card and can be used to measure two basic parameters: antenna gain and radiation pattern. Therefore, the algorithm of software in [1] is re-designed so that it can be operated on variety types of equipment, can be modified easily and can be used to measure 4 parameters with noise reduction function.

In this chapter, section 2.2 presents new software structure. The software is divided into independent modules for easy modification and change of measurement equipments. Section 2.3 presents new signal processing algorithm for noise reduction in antenna measurement. With the noise reduction function, the measurement results are more beautiful than the original ones. Four measurement parameters that can be measured by new software are gain, radiation pattern, polarization and 3D radiation pattern.

## 2.2. Improvement of software structure

### 2.2.1 Measurement configuration and new software structure

The facilities that are used to implement the algorithm consist of anechoic chamber (16 m × 8 m × 6 m, from 30 MHz to 40 GHz), signal generator (Agilent 83650L), microwave receiver (Agilent 8530A), Orbit positioners (AL-4372-1 and AL-560-1) with positioner controller (AL-4906-3A) and IBM compatible computer with GPIB interface card.

The configuration of antenna measurement system is shown in Fig. 2.1 [4]. Antenna under test (AUT) is located on azimuth/elevator (AZ/EL) positioner; transmitting antenna is located on polarization positioner or on a fixed tower, depends on a measured parameter. Antennas and positioner are in the chamber room, other equipments are out side. For automatically measuring, all equipments are controlled by measurement program via GPIB interface.

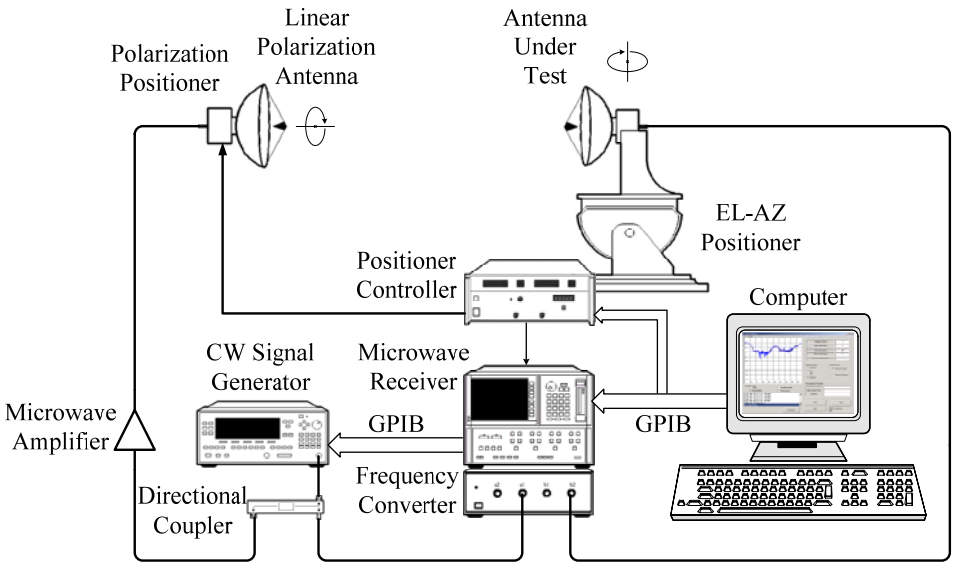


Fig. 2.1 Configuration of antenna measurement

The algorithm is designed to meet following requirements: first, can be used to measure different parameters automatically, reliably and exactly; second, equipments can be changed easily with a small modification of program; third, the program has a graphic user interface (GUI). To meet these requirements, the program is divided into 4 layers as shown in Fig. 2.2. Communications between two adjacent layers is performed via pre-defined subroutines. This structure makes the layers independent and can be modified easily.

Layer 1 performs GPIB interface. This layer is written and compiled as an independent dynamic link library (DLL) file for each type of interface card. When interface card is changed, only DLL file is changed. This algorithm makes a change of GPIB interface card easier and can be used for other interface protocol such as transmission control protocol / internet protocol (TCP/IP). This layer communicates with GPIB card via subroutines that are sup1plied by GPIB card manufacturer.

Layer 2 performs equipment interface by using command set of equipments. Equipments are controlled and data is received via this layer. Command set for equipment are stored in text files. When equipments are changed, the command set for this layer is changed by changing the command text file.

Layer 3 performs data processing. Data consists of input data from user and measurement data from equipments. Input data is processed to convert to appropriate data for sending to equipments and storing on hard disk. Measurement data is processed and manipulated to calculate the required parameters. In addition, measurement data can be processed to improve measurement results.

Layer 4 performs GUI user interface. In this layer, user can interact with measurement system such as enter measurement parameters, start/stop measuring process, view measurement results, and manage measurement data.

With this structure, above requirements are met well. Each layer is implemented as an independent module and can be modified or changed easily when equipments are changed. This structure is applied for measuring 4 parameters of antenna: gain, radiation pattern, polarization and 3D radiation pattern. Only layer 4 and layer 3 for each parameter are different. The common flow chart for measurement parameters are shown in Fig. 2.2.

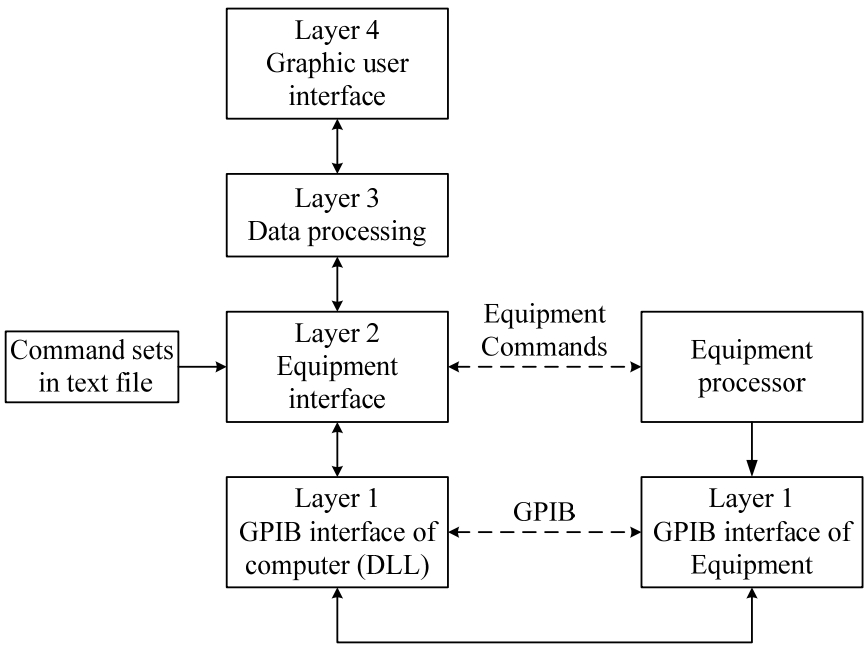


Fig. 2.2 Structure of measurement software

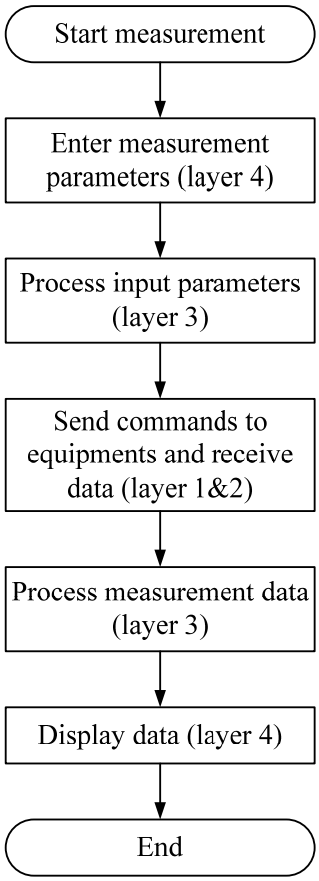


Fig. 2.3 Common flow chart of measurement program

### 2.2.2. Measurement results

Following figures show the graphic user interface of programs and measurement results. There are 4 parameters that are measured by the software with the configuration and algorithm shown in section 2.2.1. The antenna under test (AUT) is helical antenna as shown in Fig. 2.4. Its operating frequency band is 2.6 GHz ~ 3.95 GHz.

Fig. 2.5 shows radiation pattern of helical antenna at 3 GHz in polar coordinate, from 0 degree to 360 degree. To measure radiation pattern, user input measurement parameters and press start button. The system operates automatically and measurement result is displayed. User can choose polar or rectangular coordinate to display data. And the measured pattern can be normalized by choosing the mode of display.

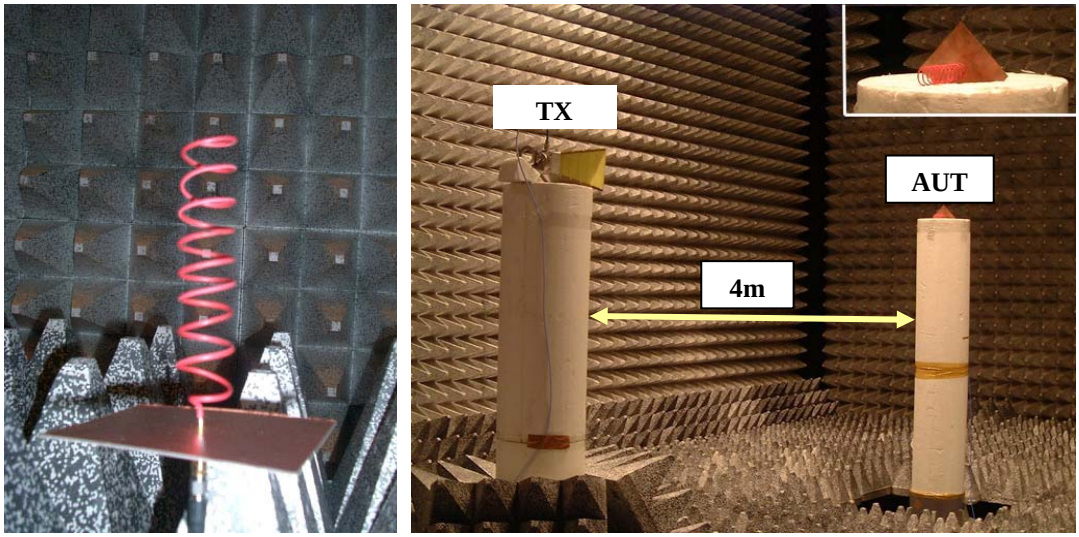


(a) AUT (b) TX antenna and AUT in anechoic chamber

Fig. 2.4 Antenna measurement

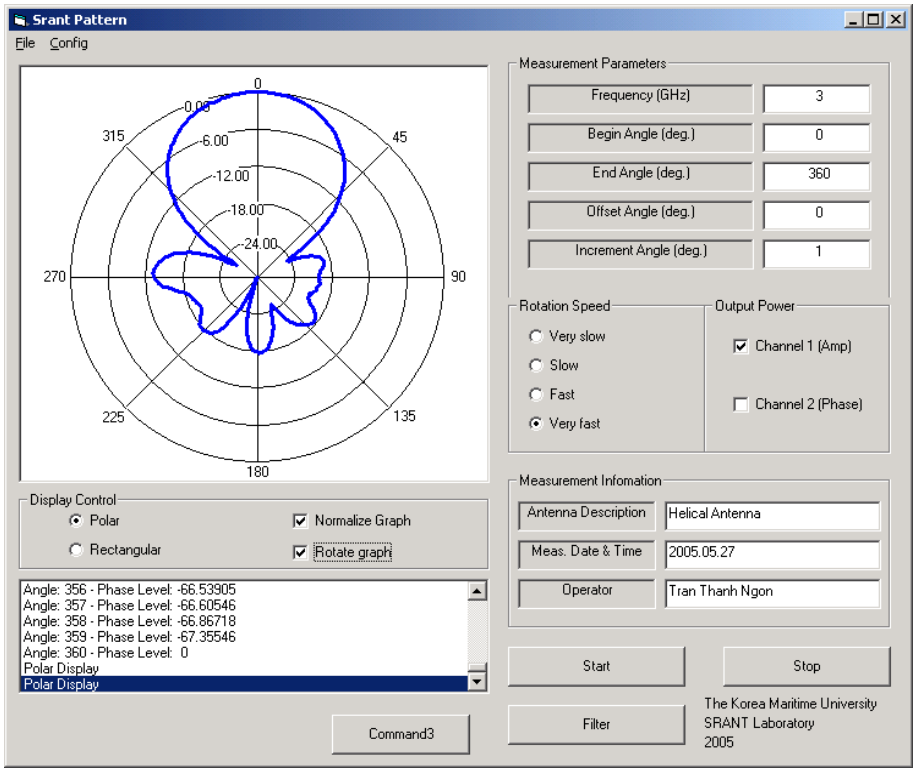


Fig. 2.5 Radiation pattern of helical antenna.

Fig. 2.6 shows gain of antenna from 2.6 GHz to 3.95 GHz in rectangular coordinate. First, user enters measurement parameters, chooses standard antenna in the list; second,

measure power that are received by standard antenna; third, measure power that are received by AUT; finally, measurement result is calculated by (2.1) and displayed. In Fig. 2.6, gain of AUT is from 7 dB to 10 dB in frequency band of 2.65 GHz ~ 3.95 GHz.

$$G_{AUT} = G_{Std} - P_{Std} + P_{AUT} \tag{2.1}$$

where $G_{AUT}$ is gain of AUT, $G_{Std}$ is gain of standard antenna, $P_{Std}$ and $P_{AUT}$ are the power that are received by standard antenna and AUT, respectively.

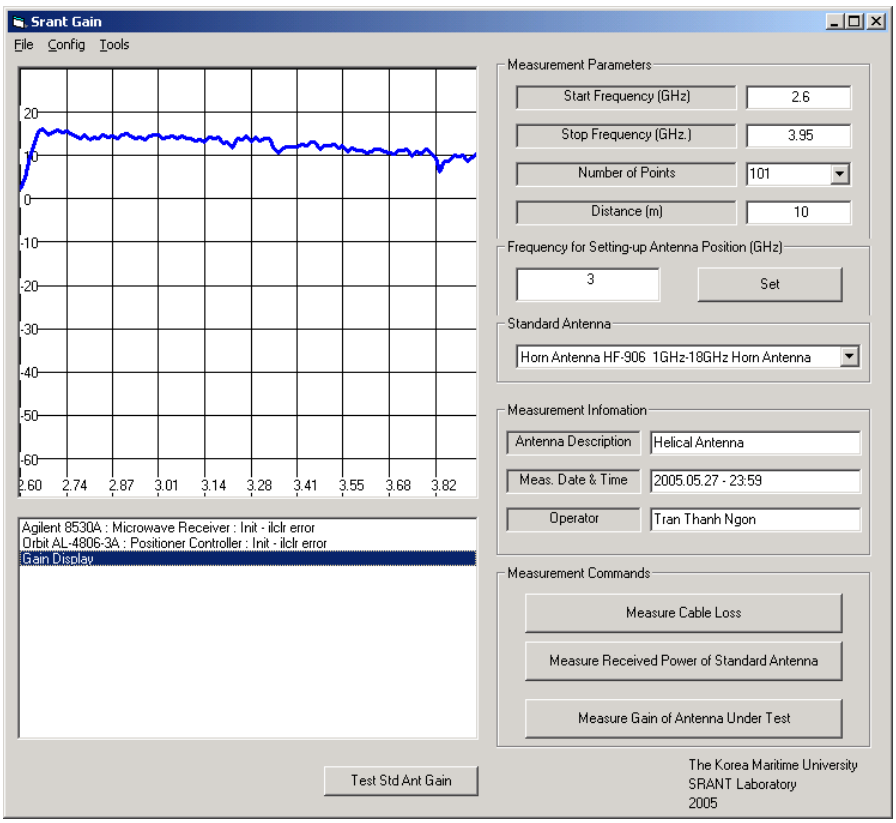


Fig. 2.6 Gain of helical antenna

Fig. 2.7 and Fig. 2.8 show results of polarization measurement of AUT. Fig. 2.7 shows magnitude of two components of E-field for AR calculation. The line 1 is magnitude of horizontal E-field ($E_{xo}$); the line 2 is magnitude of vertical E-field ($E_{yo}$). Fig. 2.8 shows result of AR calculation from (2.2)[5] with $OA$ and $OB$ in (2.3) and (2.4). The measurement data in this case consist of magnitude of two components of E-field and phase difference between two components ($\Delta\phi$).

$$AR = \frac{\text{major axis}}{\text{minor axis}} = \frac{OA}{OB} \qquad 1 \le AR \le \infty \tag{2.2}$$

where

$$OA = \left[ \frac{1}{2} \left\{ E_{xo}^2 + E_{yo}^2 + \left[ E_{xo}^4 + E_{yo}^4 + 2E_{xo}^2 E_{yo}^2 \cos(\Delta\phi) \right]^{1/2} \right\} \right]^{1/2} \tag{2.3}$$

$$OB = \left[ \frac{1}{2} \left\{ E_{xo}^2 + E_{yo}^2 - \left[ E_{xo}^4 + E_{yo}^4 + 2E_{xo}^2 E_{yo}^2 \cos(\Delta\phi) \right]^{1/2} \right\} \right]^{1/2} \tag{2.4}$$

Fig. 2.9 shows the integrated antenna measurement software. In this software, all of above functions are integrated in one GUI, include 3D radiation pattern measurement.

It is shown that with this software structure, the software can be modified easily when equipment is changed. Only a small part of program is updated or modified in this case. In addition, new algorithm for signal processing can be applied easily when signal level is low and make the measurement result more reliable and exact.

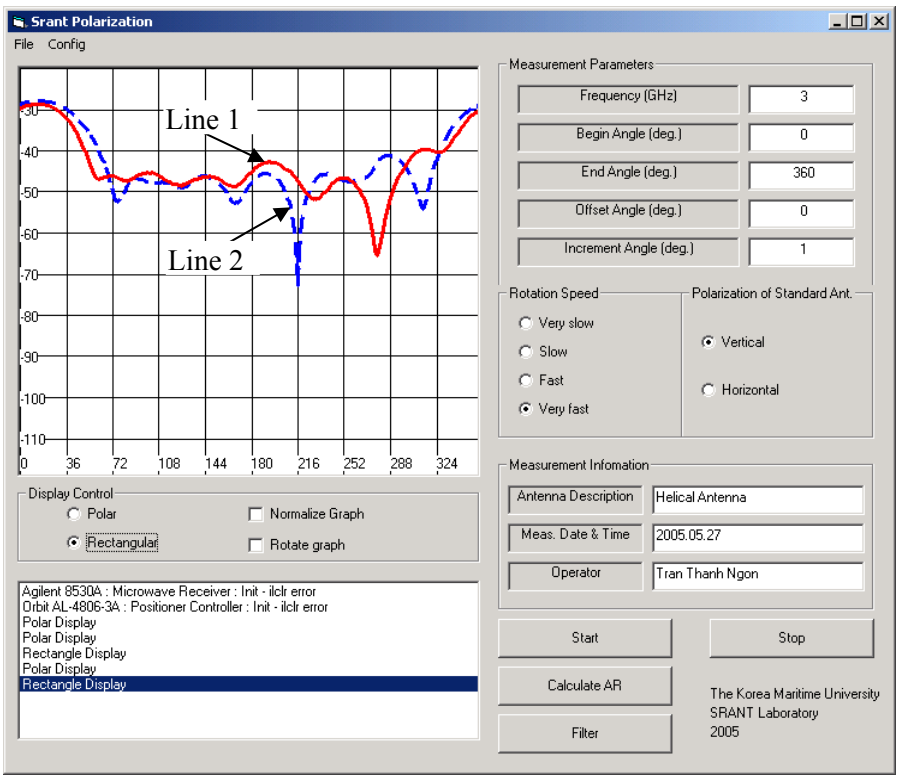


Fig. 2.7 Two components of E-field of helical antenna

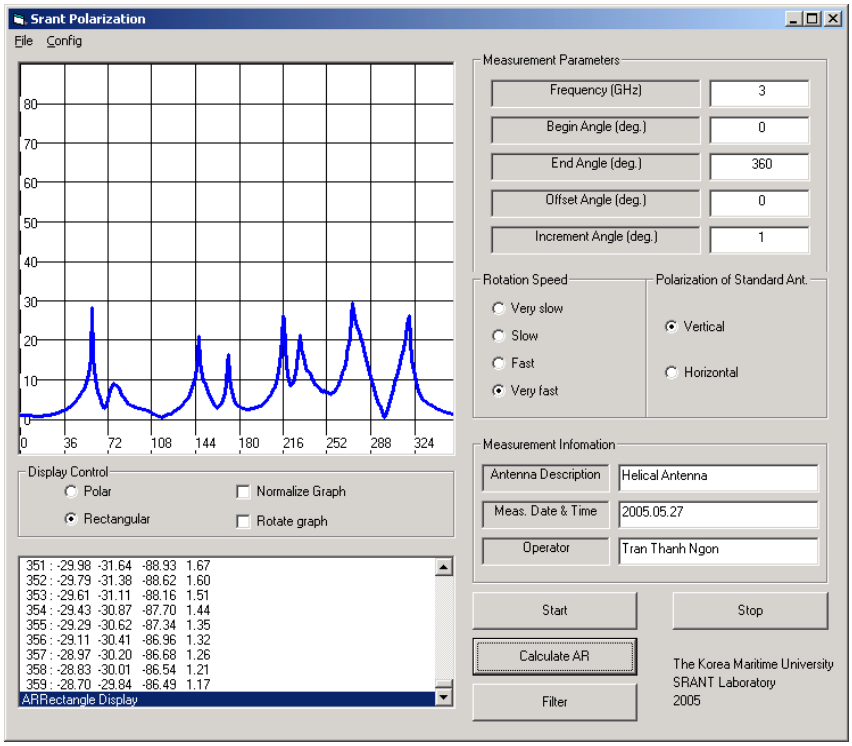


Fig. 2.8 Axial ratio of helical antenna

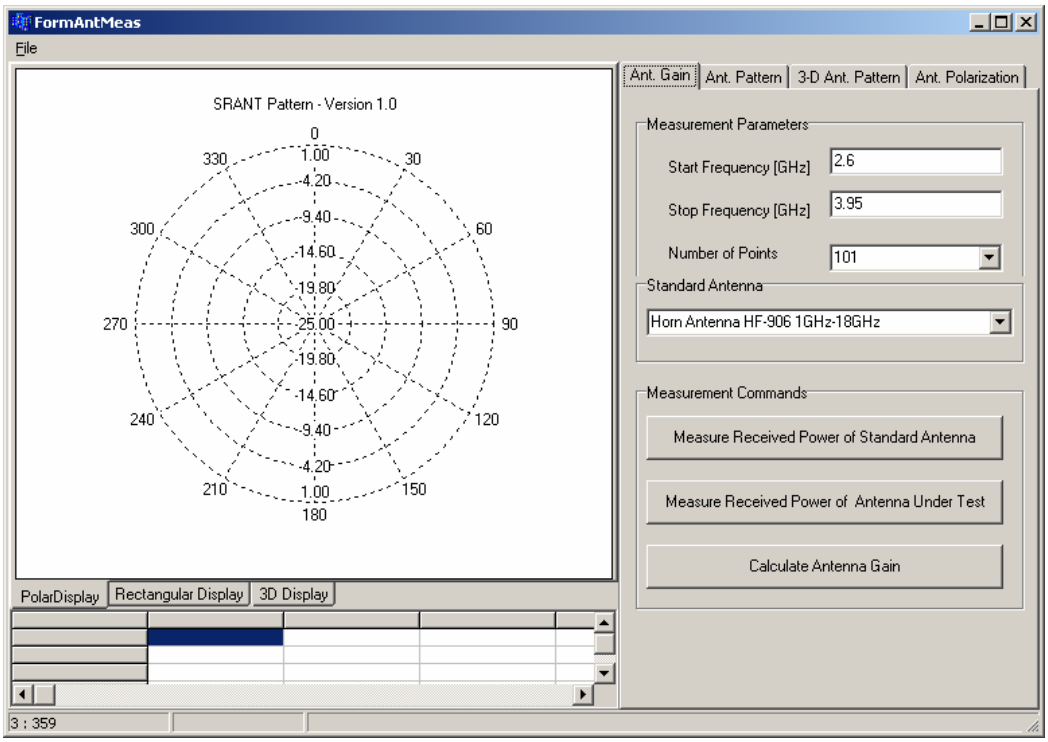


Fig. 2.9 Integrated antenna measurement software

## 2.3. Filter algorithm for noise reduction in antenna measurement

In measurement of antenna gain and radiation pattern, when level of received signal is low, measurement results are very noisy. Fig. 2.18 shows the radiation pattern of the AUT shown in Fig. 2.4. Noise causes high ripple in measurement results because of low signal to noise ratio (SNR). There are number of factors that cause this problem, such as low transmitting power level, high cable loss and propagation loss, low antenna gain as shown in Friis equation [5]. There are several methods that are used to overcome this problem, such as increase transmitting power level by adding the amplifier, reduce cable loss by using short cable (small anechoic chamber) or using up/down converter to decrease the frequency of signal on cable, using the transmitting antenna with high gain or using filter algorithms in measurement software. This thesis presents the new filter algorithm that is suggested for reducing noise with the desired error level and the optimized measurement time.

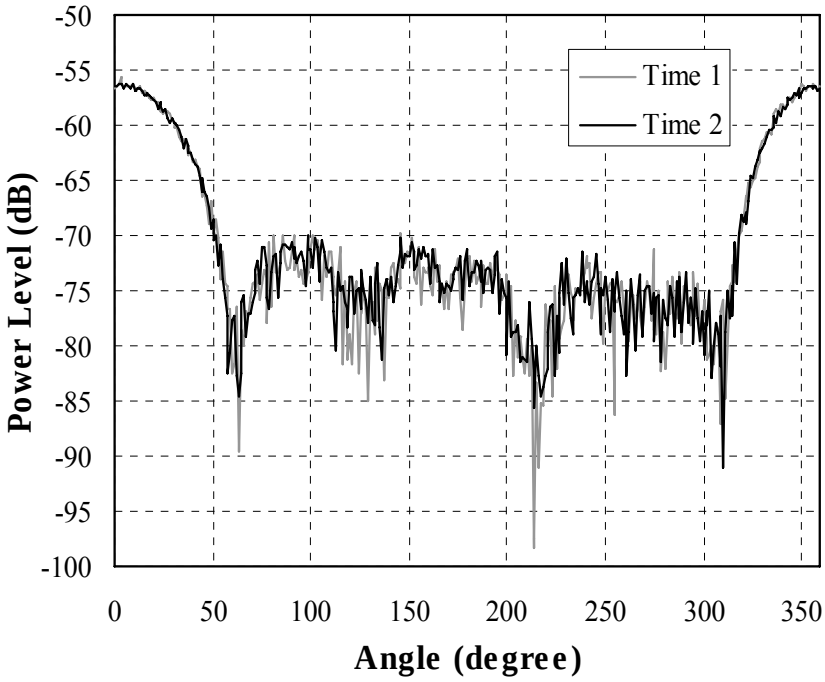


Fig. 2.10 Original signal of radiation pattern.

Because the noise in measurement systems is additive white Gaussian noise (AWGN) so the use of mean filters are suitable in this case [6]. In the measurement system shown in

[4], the time mean filter is used by calculating the average of the preseted number of samples ($N$) at one measurement point. The number of measured samples is the product of $N$ and number of measurement points, it is a large number and it takes the time for measurement. In addition, there is the smooth function in [4]. This function makes the graph smooth by calculating the average of adjacent points. It is the space mean filter. In the measurement software shown in [10], there is the weighted smooth function that calculates the weighted average of adjacent points. The smooth functions in [4] and [10] cause error, especially when noise level is high or the patterns have narrow beam width. In this chapter, the real time combination of the time adaptive mean filter (TAM) and the space adaptive mean filter (SAM) is suggested to control the measurement error and optimize measurement time. The measurement error caused by noise is considered in this algorithm, not include the equipment error. This algorithm is developed from [9]. It is the tighter combination of SAM and TAM.

SAM filter is a mean filter in which data at one point is an average value of adjacent data points. Numbers of adjacent data points in average calculation are changed adaptively, depending on the calculation point. Therefore, this filter is called SAM filter. SAM filter has best performance on the straight segments of the graph. TAM is a mean filter in which data at one point is an average value of its samples at different time instant. Number of samples is changed adaptively, depending on the noise level at the measurement point and the required measurement error. Therefore, this filter is called TAM filter.

In [9], TAM filter is implemented real-time and then SAM filter is implemented offline. Because SAM filter is implemented off line, the errors occur at the peaks or nulls of the signal, especially when the signals have narrow beam width. In addition, because TAM and SAM are implemented separately, the total of measured samples is not optimized, i.e. measurement time is not optimized. In this section, TAM and SAM filters are implemented real-time to calculate the optimum number of samples at the measurement point with the desired error level.

### 2.3.1. Filter algorithm

The receiver measures power of the received signal. The samples of signal power can be presented as (2.5) [7].

$$d[j] = D + n[j] \tag{2.5}$$

where $d[j]$ is a independent repeated measurement of signal power, $D$ and $n[j]$ are a expected power level of $d[j]$ and noise level, respectively. $d[j]$ , $n[j]$ has Gaussian distribution. The noise $n[j]$ needs to be eliminated.

In measurement of antenna gain or radiation pattern, the measurement data consists of various data points that correspond to the required frequency points or the required angle point. Therefore (2.5) can be modified as (2.6)

$$d[i, j] = D[i] + n[i, j] \tag{2.6}$$

where $i$ is the required frequency point in gain measurement or the required angle point in pattern measurement. The maximum value of $i$ is chosen by user and the maximum value of $j$ is controlled by filter algorithm. Mean and variance value of $d[i,j]$ are $D[i]$ and $\sigma[i]^2$, respectively. $D[i]$ is a required true value.

From the laws of large number [7], the sample mean of $d[i,j]$ is:

$$D'[i] = \frac{1}{N}\sum_{j=1}^{N} d[i, j] \tag{2.7}$$

The error between $D[i]$ and $D'[i]$ is $\varepsilon$

$$\varepsilon = \left|D'[i] - D[i]\right| \tag{2.8}$$

For any choice of error $\varepsilon$ and probability $1 - \delta$ the number of samples N can be selected so that $D'[i]$ is within $\varepsilon$ of true mean with probability $1 - \delta$ or greater [7].

$$P\left[\left|D'[i] - D[i]\right| < \varepsilon\right] \geq 1 - \frac{\sigma[i]^2}{N\varepsilon^2} \tag{2.9}$$

where $\sigma^2/(N\varepsilon^2) = \delta$.

In measurement, the logarithm scale is used and the error $\varepsilon$ is described in dB, $\varepsilon_{dB}$.

$$\varepsilon_{dB} = 10\log\frac{D'[i]}{D[i]} \tag{2.10}$$

Therefore, $\varepsilon$ can be calculated from $\varepsilon_{dB}$ by (2.11)

$$\varepsilon = \left|D'[i] - D[i]\right| = D[i]\left(10^{0.1\varepsilon_{dB}} - 1\right) \tag{2.11}$$

Equation (2.11) show that when $D[i]$ is high, ε is high and from (2.9), number of samples N is small.

The sample variance of noise can be calculated by (2.12)[8].

$$\sigma^2 = \frac{1}{M}\sum_{i=1}^{M}\left(s[i] - S\right)^2 \tag{2.12}$$

where $s[i]$ is a independent repeated measurement of signal power in the calibration process with the fixed measurement condition and low signal level; $S$ is the average value of $s[i]$. Number of $s[i]$ samples $M$ is as large as possible

The number of measurement samples N at one measurement point is calculated from (2.9), the sample mean $D'[i]$ is calculated from (2.7) and the error is ε. Equation (2.7) is the TAM filter as in [9]. To calculate ε from $\varepsilon_{dB}$ as in (2.11), $D[i]$ must be known. To estimate $D[i]$, the external interpolation is used with the application of SAM filter. Firstly, SAM filter is applied and then external interpolation is used to estimate $D[i]$. If $D'[i]$ is a linear function of $i$, the data at point $i$ can be calculated from the previous as follow:

First, the average slope of pattern is calculated as in (2.13).

$$\begin{aligned} SL &= \frac{1}{W-1}\sum_{j=i-W}^{i-1}\left(\frac{D'[j+1] - D'[j]}{(j+1) - j}\right) \\ &= \frac{1}{W-1}\sum_{j=i-W}^{i-1}\left(D'[j+1] - D'[j]\right) \end{aligned} \tag{2.13}$$

where W is the number of points in which the $D'[i]$ is a linear function of $i$.

Next, data value at point $i$ is calculated as in (2.14) as an average of $W$ points that are calculate from $W - 1$ previous points and the processing point with slope $SL$. $W$ is called processing window.

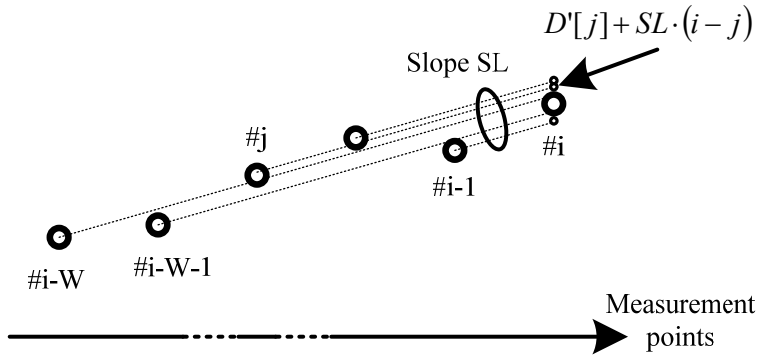


Fig. 2.11 Illustration of *D''*[i] and *SL*

$$D''[i]=\frac{1}{W+1}\sum_{j=i-W}^{i}\left[D'[j]+SL\cdot(i-j)\right] \tag{2.14}$$

Equation (2.14) is an implementation of the SAM filter. The processing window $W$ is chosen so that the difference between $D''[i]$ and $D'[j]+SL\cdot(i-j)$ is smaller than the desired error value as in (2.15).

$$\left|\left[D'[j]+SL\cdot(i-j)\right]-D'[i]\right|\le\varepsilon, \qquad i-W\le j\le i \tag{2.15}$$

With the application of (2.14), the number of samples $N$ in (2.7) become $N'$ as in (2.16).

$$N'=\begin{cases}N-W, & N>W\\ 1, & \mathrm{N}\le\mathrm{W}\end{cases} \tag{2.16}$$

From (2.7), (2.14) and (2.16), the total of samples is $N$ in average calculation of one point. It means that the condition (2.9) is satisfied. The total of measurement samples is the sum of $N'$ at all measurement points.

The next point can be estimated by external interpolation as in (2.17). This value is used for measuring and processing next point.

$$D[i+1]=D'[i]+SL \tag{2.17}$$

With this algorithm, TAM and SAM filters are implemented real-time. The results of TAM are used for SAM filter and the results of SAM filter are used for TAM filter in

measurement process. This combination of TAM and SAM filters is tighter than filter combination in [9].

The filter algorithm is implemented as following steps:

1. Calibration
2. Measure the two first points and estimate the power level to calculate number of samples as in (2.9).
3. Find $W$ by increasing W from 1 and checking the condition (2.15).
4. Calculate the average slope as in (2.13) and applied SAM filter as in (2.14).
5. Estimate next measurement point as in (2.17) and calculate next number of samples as in (2.16) and (2.9).
6. Get new samples and calculate the time average by TAM filter by (2.7).
7. Check the conditions (2.15) and (2.16). If it is not satisfied, re-calculate $W$, $N$ and go to step 6. Other wise, go to step (2.8).
8. Continue until last point.

### 2.3.2. Experimental results of filter algorithm

In this section, the radiation pattern of the helical antenna is measured and processed by using the algorithm described in section 2.3.1.

For evaluating performance of this algorithm, result of different types of mean filter are displayed and compared with reference signal. The mean filters are space mean(SM), time mean(TM), SAM, TAM and combination of TAM & SAM. TM and SM are mean filter type with fixed $N$ and $W$ respectively as in (2.7) and (2.14). The reference signal is shown in Fig. 2.12. This signal is measured and processed by TM filter with $N = 200$, i.e. there are 200 data samples at each data point. With $N = 200$, the error is lower than 0.2dB. Total of samples are $360 \times 200 = 72000$ samples and measurement time is 133 minutes (7992 seconds).

Fig. 2.13 shows results when TM filter is applied in two case: $N = 10$ and 100. With this algorithm, when $N$ is small, there is ripple at null points; when $N$ is large the signal is

smooth but number of measured samples is very large so measurement time is long. Numbers of samples are 3600 and 36000 when $N$ = 10 and 100 respectively; measurement time is 400 seconds and 3996 seconds respectively.

Fig. 2.14 shows filter results when SM filter is applied in two case: $W$ = 5 and 9. With this algorithm, when $W$ is small the signal is not smooth and there error at null points; when $W$ is large the signal is smoother but it cause big error at null points and peak points. Number of samples in two cases are 360 and measurement time is 40 seconds. When these results are compared with reference signal, error is higher than TM cases.

In Fig. 2.15, result of TAM filter is displayed. The result matches reference signal well and there are ripples. In this case, number of samples is 15000 and measurement time is 1665 seconds. The result is better than result of TM filter $N$ = 100 and measurement time is shorter.

The signal in Fig. 2.16 is the filter result when SAM filters is applied. With this algorithm, number of measured sample is 360 and measurement time is 40 second. There is big variation at null points but smooth else where. The result does not match well the reference signal. This problem depends on noise status at measurement time.

Therefore, if TAM and SAM filters are combined together, the result is better. TAM result matches well the reference signal but measurement time is long and there is no high ripple at null points, while SAM filter makes smooth result except at null points and measurement time is short. Fig. 2.17 shows measurement result with the application of the improved algorithm. Total of measurement samples in this case is 7000 samples and the corresponding measurement time is 777 seconds. Compare with the un-processed signal, this pattern is very clear and there is small ripple, especially at nulls.

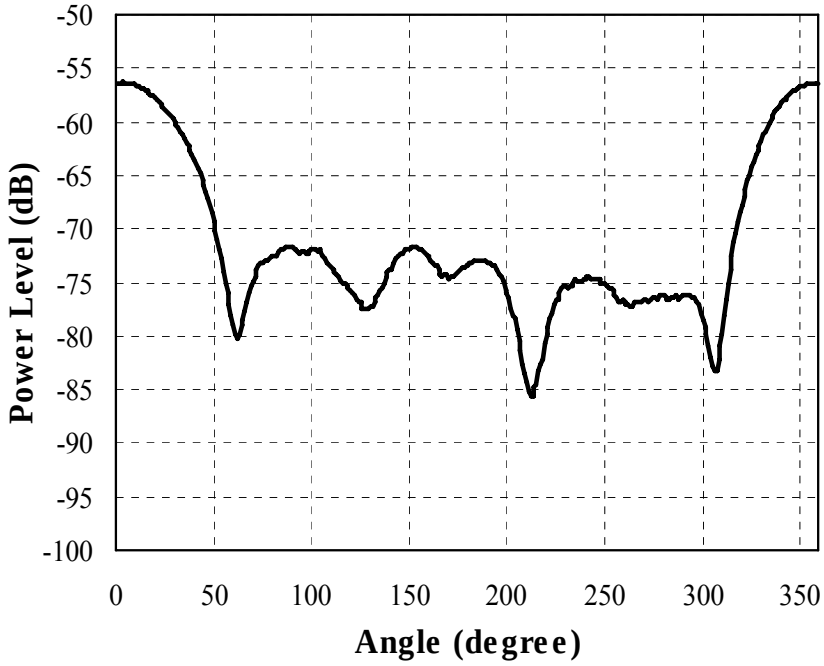


Fig. 2.12 Reference signal.

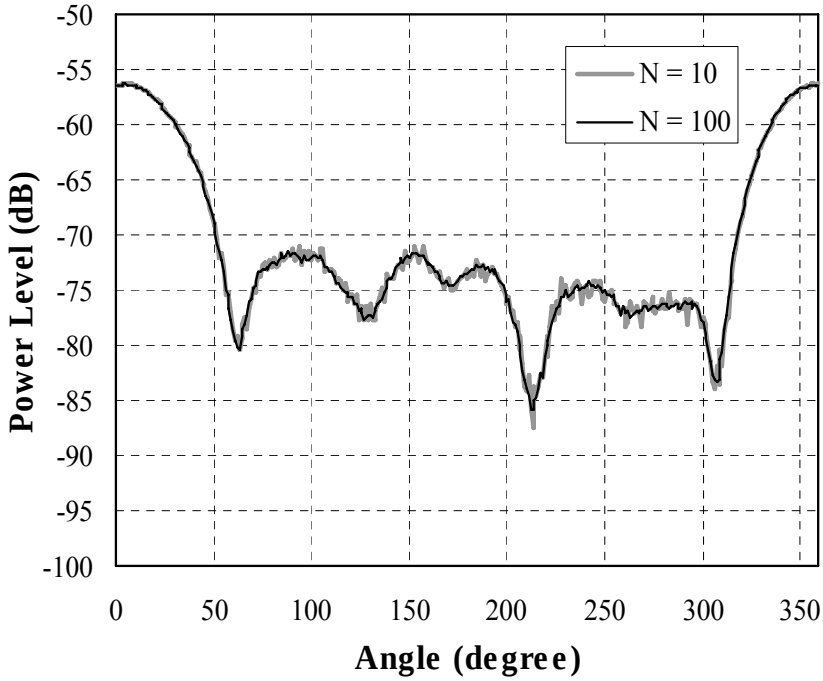


Fig. 2.13 Signal filtered by TM filter $N = 5$ & 150

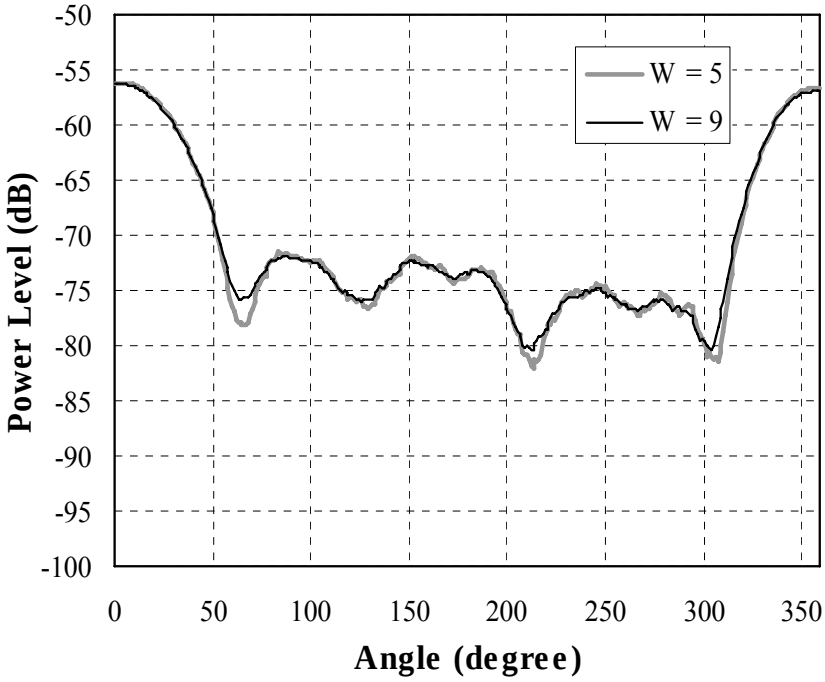


Fig. 2.14 Signal filtered by SM filter $W = 5$ & 9.

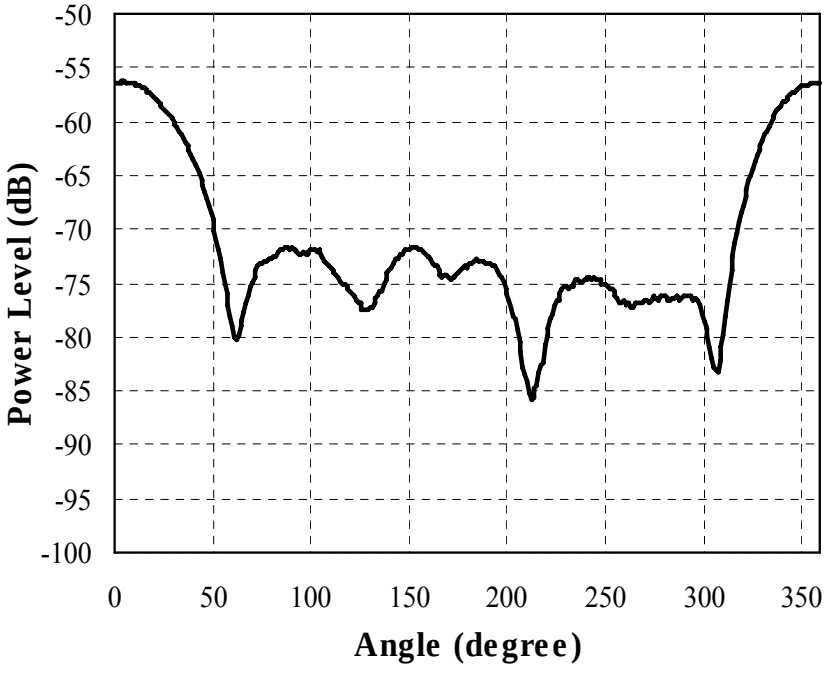


Fig. 2.15 Signal filtered by TAM filter.

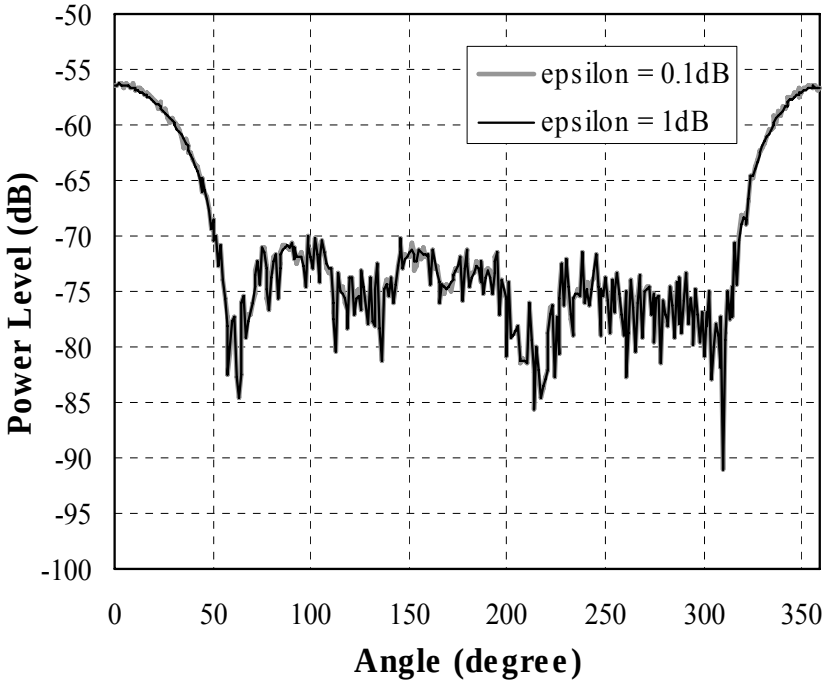


Fig. 2.16 Signal filtered by SAM filter.

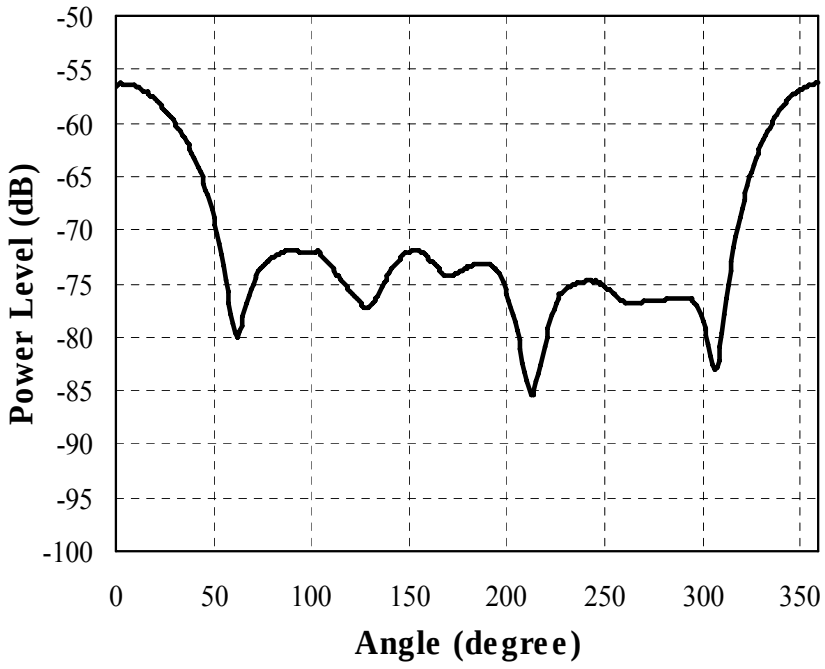


Fig. 2.17 Filtered signal

## 2.4. Summary

The algorithm of the antenna measurement software is improved. With this algorithm, the software can be operated on variety types of equipment, can be modified easily and can measure 4 parameters with noise reduction function. Four parameters are antenna gain, 2-D radiation pattern, 3-D radiation pattern and polarization. In addition, the filter algorithm is developed for reducing measurement noise. With the application of the filter algorithm, the measurement time and error are improved. The tight combination of TAM filter and SAM filter is used to optimize the number of measurement samples, i.e. measurement time. Because the conditions (2.9) and (2.15) are satisfied, the error is kept within the desired value. This algorithm is implemented in the practical measurement system and yield the good result. The high ripples at nulls are removed. The result is more reliable.

# CHAPTER 3

# MEASUREMENT OF KEY PARAMETERS OF MIMO ANTENNA

## 3.1. Objective

In mobile radio communication links, it is realized that when number of antennas is increased at one end, capacity of channel can be increased [11]. This increase is the result of array antenna diversities and makes MIMO antennas suitable for multi-media mobile communication. Functional blocks of MIMO systems consist of transmission channel, antennas, and signal processing unit.

MIMO antenna consists of several antenna elements. Number and size of elements depend on operating frequency and applications in which MIMO antenna is used. Antenna diversity is created by the use of multiple antennas. Diversity is one of important characteristics of MIMO antennas. With good diversity performance, radio wave can be received or transmitted well in any direction with any kind of polarization and correlation coefficients of received signals from antenna elements are low. Therefore, the channel capacity is increased. To achieve good diversity performance, MIMO antennas have to satisfy following characteristics: have enough directivity gain, suitable level of cross-polarization discrimination (XPD), differently directed spatial radiation patterns, minimum mutual coupling, small size and matched terminals [12].

In design and measurement of MIMO antennas, above characteristics are required to evaluate performance of antenna. In this chapter, the practical measurement of pattern (gain) diversity, polarization diversity, pattern correlation and mutual coupling are presented with discussion. The improved measurement software presented in chapter 1 is used to measure these parameters of MIMO antenna.

## 3.2. Measurement configuration

Measurement system in fig. 2.1 is used for this measurement. EUT is mounted on elevation–azimuth positioner. The sample of EUT used to test the measurement is a copper box with the size of personal data assistants (PDA) as shown in Fig. 3.2. The copper box is also used as a ground plane of antenna elements. EUT has 4 antennas elements that are numbered as in Fig. 2(a) and center operating frequency of 5.2 GHz. When one element is measured, other ones must be terminated by 50Ω-terminator.

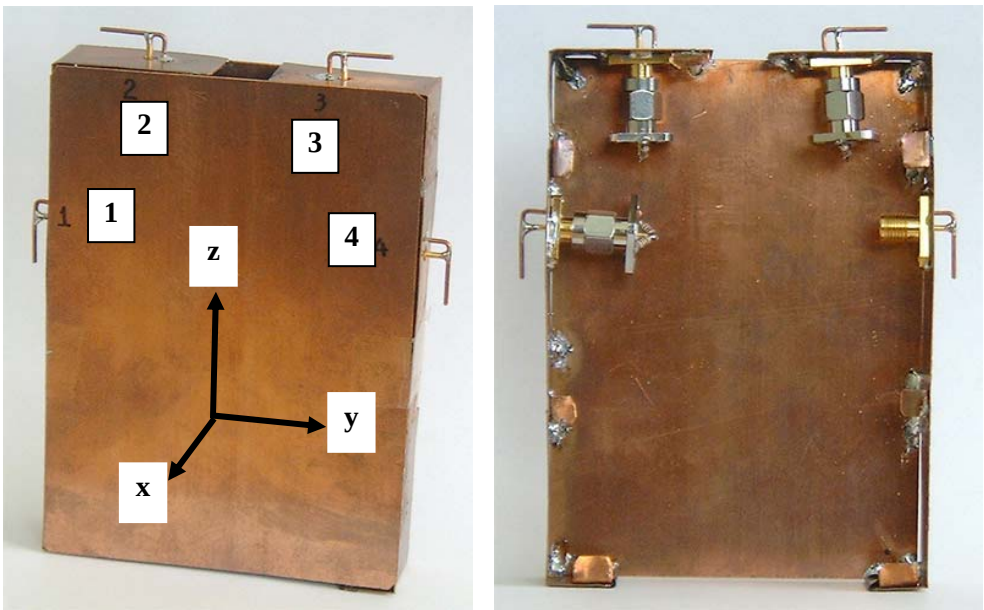


(a) Front view (b) Inside

Fig. 3.2 Sample of EUT (PDA size 75×110×7 mm)

### 3.2.1 Pattern diversity, polarization diversity and calculation of pattern correlation

Measurement of pattern diversity and polarization diversity are taken independently on each element. Techniques used for measuring pattern and polarization are referred in [13]. The result patterns are evaluated.

It is realized that MIMO antennas with low pattern correlation coefficient have good diversity performance [12]. In this chapter, the correlation of patterns on measurement planes are calculated and evaluated. There are three measurement planes, such as x-y plane,

x-z plane and y-z plane. In each plane, there are two components of E field, $E_\theta$ and $E_\phi$. Correlation coefficient of two patterns in same plane and polarization is calculated by using (3.1) [14].

$$\rho_c = \left| \frac{\sum_{i=0}^{359} (E_1[i] - \overline{E}_1)(E_2[i] - \overline{E}_2)}{\sqrt{\sum_{i=0}^{359} (E_1[i] - \overline{E}_1)^2 \sum_{i=0}^{359} (E_2[i] - \overline{E}_2)^2}} \right| \tag{3.1}$$

where $E_1$ and $E_2$ are data series of E-field patterns and $\overline{E}_1, \overline{E}_2$ are the average value of $E_1$ and $E_2$ respectively. Number of data points is 360.

### 3.2.2. Measurement of mutual coupling

Mutual coupling between antennas is caused by the radiated field of antennas and the induced current on the ground surface of two adjacent antennas. In MIMO antenna systems, when all antenna elements operate simultaneously at same frequency, mutual coupling causes antenna impedance and radiation pattern to be changed. The good MIMO antennas have mutual coupling below -20 dB [12]. Mutual coupling is measured by using network analyzer.

## 3.3. Results and discussions

### 3.3.1 Pattern diversity and polarization diversity

Patterns and polarizations of EUT antenna elements are measure at the frequency of 5.2 GHz. Transmitting antenna is the horn antenna with gain of 10.9 dBi at 5.2 GHz. Distance between transmitting antenna and EUT is about 2 m. Four antenna elements are measured independently in 3 planes such as x-y plane, x-z plane and y-z plane.

Fig. 3.3, 3.4, 3.5 and 3.6 are the relative received signal level of antenna element #1, #2, #3, and #4 respectively with same measurement conditions. E-theta ( $E_\theta$ ) and E-phi ( $E_\phi$ ) are two components of E field in each plane.

The XPD of EUT antenna elements on three planes can be calculated from the received signal level in Fig. 3, 4, 5 and 6 by using (3.2)[15]

$$XPD = 20\log\frac{E_{co}}{E_{cross}} = E_{co[dB]} - E_{cross[dB]} \tag{3.2}$$

where $E_{co}$ and $E_{cross}$ are co-polarization and cross-polarization components of E-field, respectively. Fig. 3.3(b) and 3.6(b) show that antenna elements #1 and #4 have horizontal linear polarization while Fig. 3.4(a) and 3.5(a) show that antenna elements #1 and #4 have vertical linear polarization because XPD is higher than 20 dB. Two pairs of antenna elements (#1 & #4 and #2 & #3) have different polarization with high XPD, for example, the difference of E-theta in Fig. 3.3(a) and 3.4(a) is about 20 dB, so the polarization diversity is good.

Fig. 3.3(b), 3.4(b), 3.5(b) and 3.6(b) show that the received power of E-theta is very low in z direction because the polarization of four elements is mismatched. To overcome this problem, one element can be placed on back of EUT, for example element 3 can be moved to back of EUT.

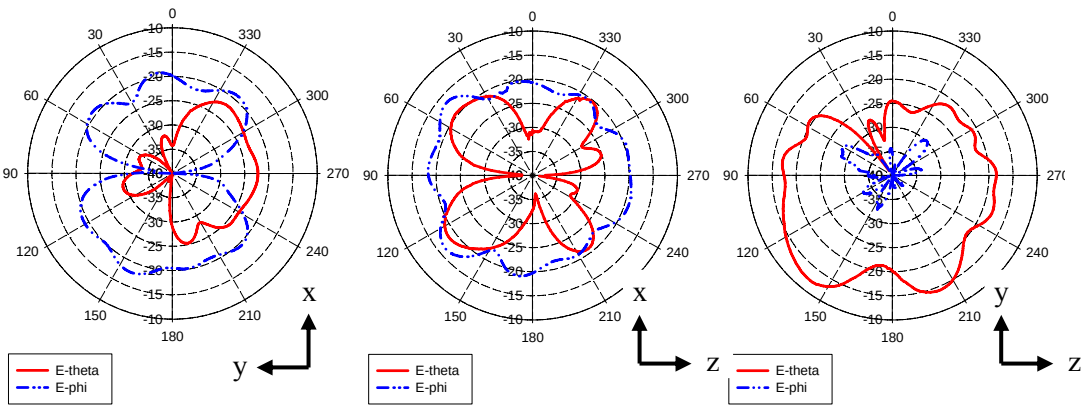


Fig. 3.3 Radiation pattern of element #1 - (a) x-y plane, (b) x-z plane, (c) y-z plane

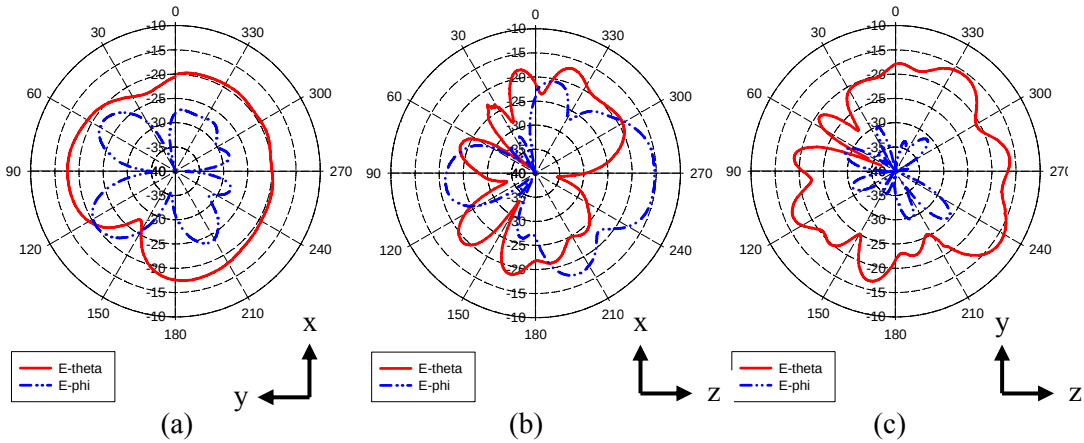


Fig. 3.4 Radiation pattern of element #2 - (a) x-y plane, (b) x-z plane, (c) y-z plane

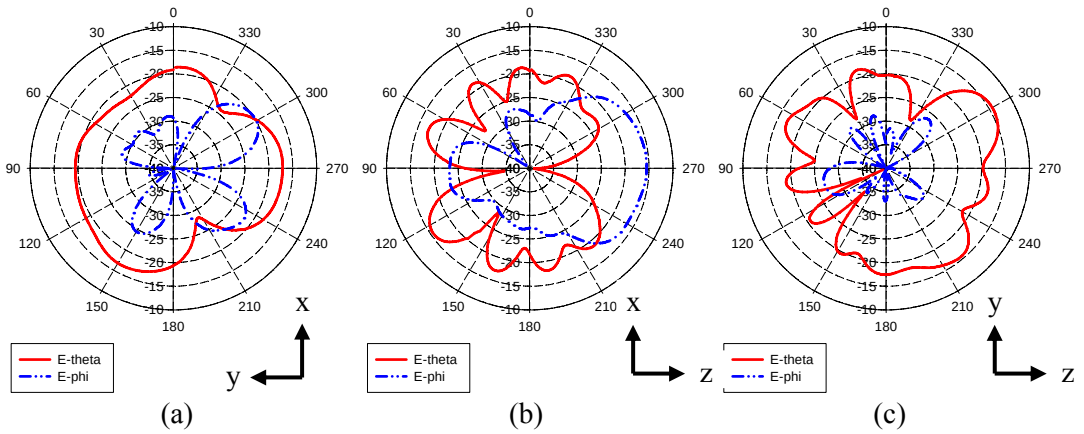


Fig. 3.5 Radiation pattern of element #3 - (a) x-y plane, (b) x-z plane, (c) y-z plane

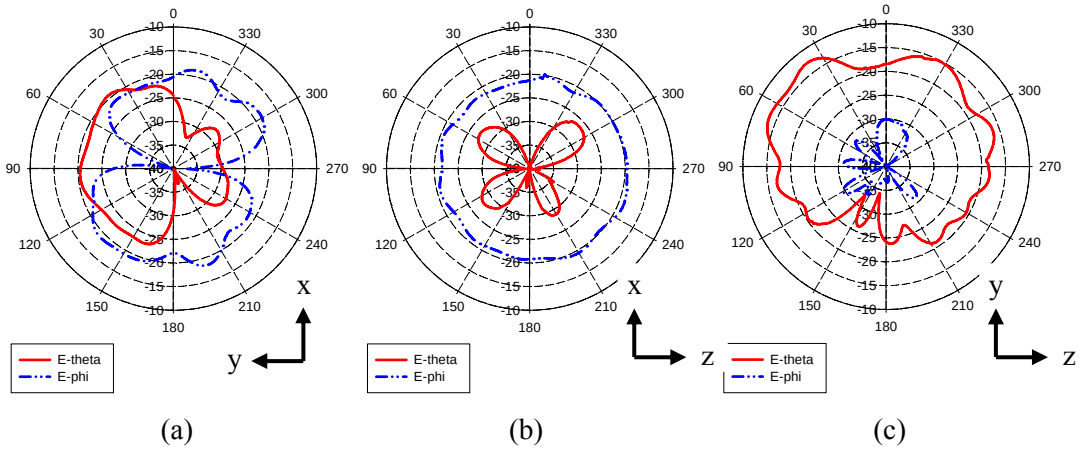


Fig. 3.6 Radiation pattern of element #4 - (a) x-y plane, (b) x-z plane, (c) y-z plane

### 3.3.2. Pattern correlation

Correlation coefficients of $E_\theta$ and $E_\phi$ patterns in measurement planes are listed in table 3.1. It is shown that the correlation coefficients on x-y plane and y-z plane are low because of different direction of antenna elements. The correlation coefficients on x-z plane are high because of same direction of antenna elements (element #1 versus #4 and element #2 versus #3), especially correlation coefficients of element #2 and #3 on this plane. This is not good for pattern diversity. To overcome this problem, a suggested alternative is to move element 3 to the back of EUT.

Table 3.1 pattern correlation of antenna elements on measurement planes

| Elements | $E_\theta$ | | | $E_\phi$ | | |
|---|---|---|---|---|---|---|
| | x-y plane | x-z plane | y-z plane | x-y plane | x-z plane | y-z plane |
| #1 and #2 | 0.103 | 0.426 | 0.022 | 0.331 | 0.222 | 0.175 |
| #1 and #3 | 0.152 | 0.481 | 0.260 | 0.071 | 0.131 | 0.269 |
| #1 and #4 | 0.100 | 0.616 | 0.352 | 0.382 | 0.607 | 0.073 |
| #2 and #3 | 0.486 | 0.822 | 0.198 | 0.107 | 0.847 | 0.027 |
| #2 and #4 | 0.196 | 0.616 | 0.085 | 0.186 | 0.118 | 0.244 |
| #3 and #4 | 0.147 | 0.543 | 0.270 | 0.110 | 0.343 | 0.139 |

### 3.3.3. Mutual coupling

Measurement method for mutual coupling is explained in section 3.2.2. Because of symmetry of EUT, only 4 parameters are measured as follow: $C_{12}$ , $C_{13}$ ,$C_{14}$ *and* $C_{23}$ .Fig. 3.7 shows the coefficient between antenna elements.

It is observed that the coupling between element #2 and #3 is the highest. This is a result of short distance between two elements and same polarization. A short distance (shorter than λ/2) causes high coupling because of the induced current on ground surface and the radiated near field. Coupling between element #1 and #2 (or element #4 and #3) is a second high one. This result is depended on the polarization diversity. Coupling between element #1 and #3 (or #4 and #2) is similar second case in mechanism and distance is longer so coupling level is lower.

From measurement results of mutual coupling, it can be concluded that to reduce mutual coupling, induced current on ground plane and polarization matching have to be reduced.

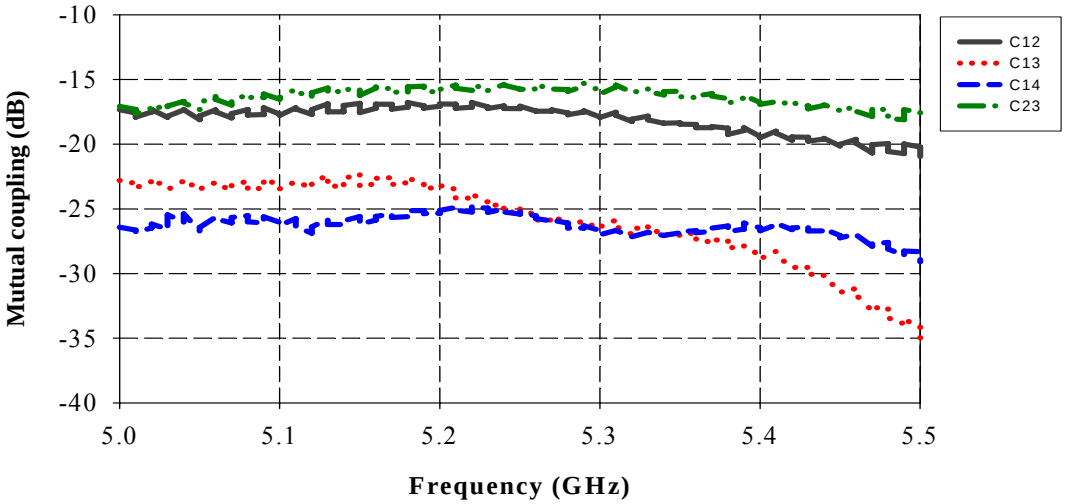


Fig. 3.7 The coupling coefficient between antenna elements

## 3.4. Summary

This chapter focuses on measurement of MIMO antenna characteristics such as gain diversity, polarization diversity and mutual coupling. These parameters are measured and calculated by using improved measurement software on practical measurement system with a sample of EUT. The results show that EUT has good pattern diversity and low pattern correlation coefficients. Polarization diversity is good with high XPD, above 20 dB, except x-directed E field in z direction. The coupling level between adjacent elements is not low enough; the required level must be below -20 dB. From the measurement results, diversity performance of MIMO antenna is evaluated and modified version of EUT are suggested to archive better antenna characteristics. These results of measurement and evaluations are useful for MIMO antenna designer in improvement of antenna characteristics.

# CHAPTER 4

# DESIGN OF MULTI-BAND MIMO TESTBED

## 4.1. Objective

As stated in [3] and in chapter 3, multiple antenna systems are of significant interest to the wireless communication community because of the increase they offer in throughput and reliability. In chapter 3, three parameters of MIMO antenna are measured and evaluated by using the antenna measurement system in chapter 1. These parameters are pattern and polarization diversity, pattern correlation and mutual coupling. These parameters are measured independently of MIMO systems that consist of transmission channel, antennas, circuits and signal processing algorithm. To evaluate other parameters of MIMO antennas on MIMO system such as antenna type, spacing, configuration, number of elements [16]… the MIMO testbed is needed. In addition, in MIMO research, theory and simulations typically show the corresponding gains under ideal conditions, hardware platforms and testbeds are essential in validating these gains in real channels and in the presence of implementation impairments [3]. Therefore, this chapter presents the design of MIMO testbed for MIMO measurement.

From [3], the block diagram of the MIMO testbed basically consists of transmitter and receiver. A transmitter consist of signal processing unit, digital to analog converter (DAC) and analog TX circuit; a receiver consists of analog RX circuit, analog to digital converter (ADC) and baseband processing unit. Fig. 4.1 shows a block diagram of MIMO testbed.

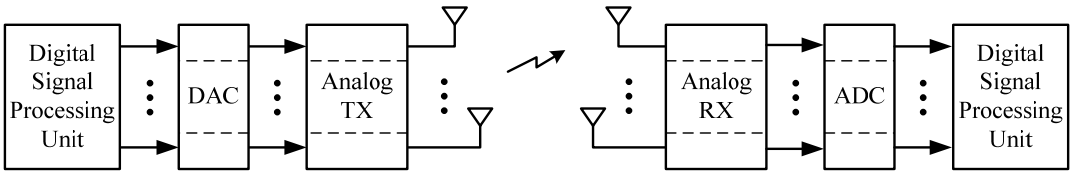


Fig. 4.1 A block diagram of MIMO testbed

The operating frequency of MIMO testbed depends on analog TX and analog RX circuits. For the flexibility of this MIMO testbed, the multi-band analog TX and RX circuits are suggested. Because wireless communication frequencies are 1.8 Ghz (cellular phones), 1.9 (PCS) GHz, 2.3 Ghz (Wibro/WiMAX), 2.4 Ghz (802.11b/g), 3.5 Ghz (802.16), 5 GHz (TriBand), 5.2 GHz (802.11a), 5.6 GHz (802.11a), 5.8 GHz (802.11a), the operating frequency range of the designed analog TX and RX circuits is 1.8 GHz – 5.8 GHz. For circuit simplification and multimode operation, direct conversion techniques are applied in design of analog TX and RX circuits and these circuits are coupled with the baseband digital signal processing unit [17]. The DAC, ADC and signal processing units are the equipment from Brains Co. and personal computer (PC). Table 4.1 shows the specifications of DAC, ADC and signal processing units

Table 4.1 Specifications

| | | |
|---|---|---|
| ADC | Channel | 16 |
| | Resolution | 12 bits |
| | Sampling rates | ~ 40 MHz |
| DAC | Channel | 16 |
| | Resolution | 14 bits |
| | Sampling rate | ~ 125 MHz |
| FPGA | 5 boards | APEX20K600<br>600K gates × 5<br>= 3000K Gates |
| CPU | HITACHI SH4 | 200 MHz, 360 MIPS,<br>1.4 GFLOPS |
| | OS | NetBSD |
| User interface | Ethernet | 100 BaseT |

In this chapter, section 4.2 presents the design of analog RX circuit; section 4.3 presents the design of analog TX circuit and section 4.4 presents the design of a 2×2 MIMO measurement system.

## 4.2. Design of analog RX circuit

In references [17] and [18], it is stated that multimode mobile terminals such as software-defined radios have been extensively researched and used. Direct conversion architectures that convert RF signals directly to baseband signals have the potential to achieve such terminals, because they eliminate the need for non-programmable image-rejection filters and IF channel filters, and perform the channel filtering at the baseband with digitally-programmable filters. Since multimode mobile terminals must be able to deal with various radio frequencies and various bit rates, they must have a wideband RF stage and programmable channel filters [17]. In addition, these terminals require a highly integrated and low-power circuit so the circuits are as simple as possible.

The direct down-conversion receivers mainly consist of LNA, quadrature down-converter, ADCs and DSP unit. For wideband multi-channel receiver, LNA and quadrature-down converter must have the wide bandwidth. Even though, it is easy to get the wide bandwidth devices, such as single chip LNA and mixers in quadrature down-converter. It is the different problem to get the simple wideband $90^o$ phase shifter in quadrature down-converter. The image signal attenuation depends on the phase and amplitude balance of quadrature down-converter. The conventional converter has 1-$5^o$ and 1-5% imbalance coefficient with about 20-40 dB image attenuation [17]. The standard Schiffman phase shifters are designed by using the coupled transmission lines and have very wide bandwidth [20], but they are difficult to realize [21], [22]. In [19], the wideband $90^o$ phase shifter was designed by using the lump circuits with phase ripple of $5^o$. To extend the bandwidth of quadrature down-converter, this paper proposes the method to extend the bandwidth of quadrature down converter by using the simple transmission line phase shifter with higher imbalance coefficient and signal processing algorithm in DSP unit. In this paper, the theoretical analysis is presented in sections 2; the simulation, fabrication and measurement results with discussions are presented in sections 3 and 4.

### 4.2.1. Receiver Architecture and Signal Analysis

Fig 4.2 shows architecture and signals in the direct down-conversion receiver. To generate in-phase (I) and quadrature (Q) signals, it is necessary to have a 90° phase shift

between the local oscillator (LO) signals (point A) or between the input signal branches (point B). In this paper, point A is considered. The ideal case is that the signals at point A are – $sin(2\pi f_C t)$ and $cos(2\pi f_C t)$. In Fig 4.2, the $g$ and $\phi$ are amplitude and phase imbalance coefficients, respectively, and these terms include the effect of baseband amplifier, low pass filter (LPF) and analog to digital converter (A/D).

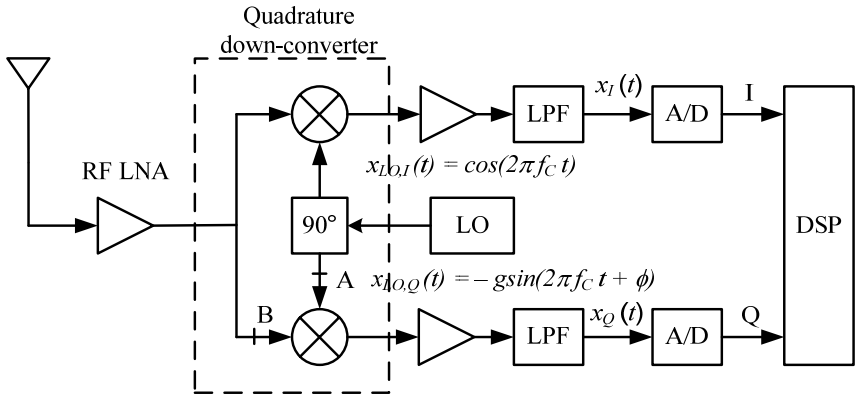


Fig. 4.2 Receiver architecture and signals in direct down-conversion receiver

In the ideal case, when the quadrature down-converter is perfectly balanced, output signals are:

$$x_I(t) = z_I(t) \tag{4.1}$$

$$x_Q(t) = z_Q(t) \tag{4.2}$$

where $z_I(t)$ and $z_Q(t)$ are the output signal in the ideal case.

Otherwise, in the case of imbalance, the output signals are expressed as:

$$x_I(t) = z_I(t) \tag{4.3}$$

$$x_Q(t) = g\cos(\phi) z_Q(t) - g\sin(\phi) z_I(t) \tag{4.4}$$

When $g$ and $\phi$ are measured, $x_Q(t)$ can be calculated as in (4.5) and (4.6).

From (4.4):

$$z_Q(t) = \frac{1}{g\cos(\phi)} x_Q(t) + \frac{\sin(\phi)}{\cos(\phi)} z_I(t) \tag{4.5}$$

And from (4.3) and (4.5):

$$z_Q(t) = \frac{1}{g\cos(\phi)} x_Q(t) + \frac{\sin(\phi)}{\cos(\phi)} x_I(t) \tag{4.6}$$

Equation (4.6) shows that $z_Q$ can be obtained from base-band signal $x_I$ , $x_Q$ and imbalance coefficients of $g$ and $\varphi$. Fig 4.3 shows the implementation of (6) in the DSP unit.

From Fig. 4.2, it is shown that baseband analog signals $x_I(t)$ and $x_Q(t)$ are quantized, converted to digital signal and processed by DSP algorithm of (4.6). The output signals are $z'_I$ and $z'_Q$ . They are different from $z_I(t)$ and $z_Q(t)$ because of quantization noise. The signal to quantization noise (SNR) of ADC is calculated by (4.7) [23] with the assumption of no aperture jitter in ADC.

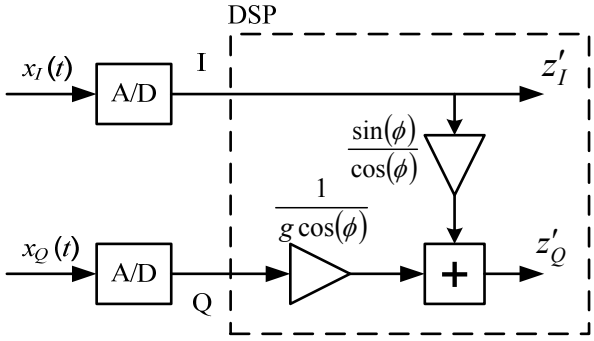


Fig. 4.3. Implementation of algorithm in DSP unit

$$SNR_{ADC} = 6.02b + 16.81 - 10\log_{10}\left(\frac{R_{FS}^2}{\sigma_x^2}\right) \tag{4.7}$$

where $b$ and $R_{FS}$ are the bit number and the full scale range of ADC, respectively, the term $\sigma_x^2$ is the input signal variance. From (4.4), when quadrature down-converter perfectly balances, the $SNR_{ADC}$ of $x_Q(t)$ and $z_Q(t)$ are the same. In the case of imbalance, the $SNR_{ADC}$ of $z_Q(t)$ are reduced by the factor of $gcos(\varphi)$.

In the good balance case, when $z_Q(t)$ is a full scale sinusoidal input and its frequency is one haft of sampling frequency (the worst case), the signal to quantization noise is calculated by (4.8) [24]:

$$SNR_{ADC} = 6.02b + 1.76 \tag{4.8}$$

With 12-bit ADC, $SNR_{ADC}$ is 74 dB.

In the case of imbalance, for example, when $g = 1$ and $\phi = 70^o$, the $SNR_{ADC}$ is reduced 4.6 dB, i.e. $SNR_{ADC}$ = *69.4 dB*. From [25], it is shown that the channel capacities are unchanged when the overall SNR are 3, 7, 11, 15 and 17 dB for 2, 4, 8, 16 and 32-PSK signal, respectively. Therefore, the effect of $SNR_{ADC}$ on overall SNR can be chosen so that the channel capacity is unchanged. From above example, $g = 1$ and $\phi = 70^o$ can be chosen because of high $SNR_{ADC}$ for 4-PSK signal with SNR of 7 dB.

### 4.2.2. Simulation and Measurement Results

Fig 4.4 shows ADS model of analog front-end circuit of the converter. In this circuit, the simple phase shifter is used to show that the bandwidth can be extended when the imbalance coefficients are increased. The phase shifter is a transmission line TL1 with resistive power divider. The resistive power divider is used to ensure that the return loss of the circuit becomes low over a wide bandwidth and phases at the outputs are equal. PORT1 and PORT2 are RF and LO sources, respectively, of the circuit. The LNA is not included because it dose not affect balance characteristics of receiver. Parameters of Mini Circuits MCA1-60 mixer chip are used in simulation. For calculation of imbalance coefficients, a RF signal with single 1 MHz baseband is used. The baseband amplifier with 40 dB gain and Butterworth low pass filter are used for baseband amplification and filter.

The simulated parameters are the S parameters of phase shifter, amplitude and phase imbalance coefficients. The simulation results are displayed and compared with measurement results in the following figures.

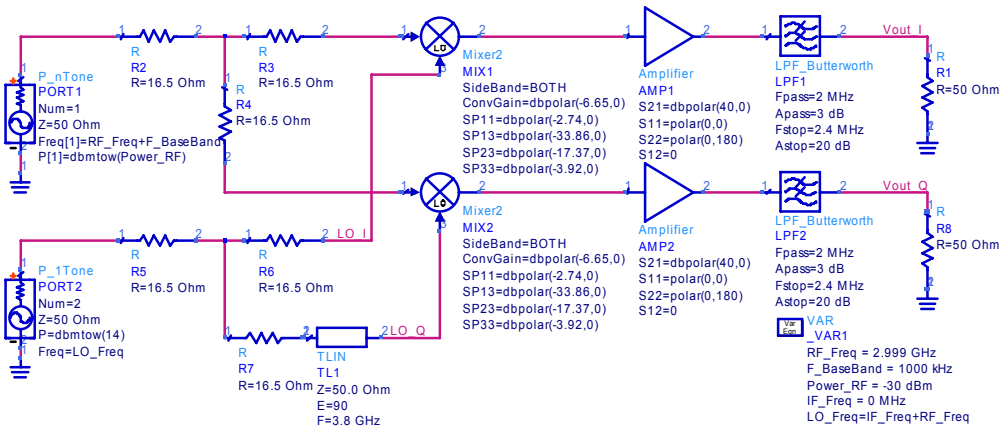


Fig 4.4 ADS model of analog front-end circuit

Fig 4.5 shows the fabricated circuits of analog part. For measurement, the analog part is divided into 4 circuits and fabricated separately. These circuits are RF power divider, mixer, LO phase shifter and baseband amplifier. The high frequency circuits are fabricated on Teflon PCB with thickness of 0.8 mm and $\varepsilon_r$ of 2.6. For the wide band operation, Mini Circuits MCA1-60 mixer chips are used. These chips have RF and LO frequency range of 1.6-6.0 GHz and IF frequency range of DC-2.0 GHz. The required LO input power of MCA1-60 is +7 dBm. The high frequency operational amplifier (OP-AMP) chips are used in the based band filter and amplifier.

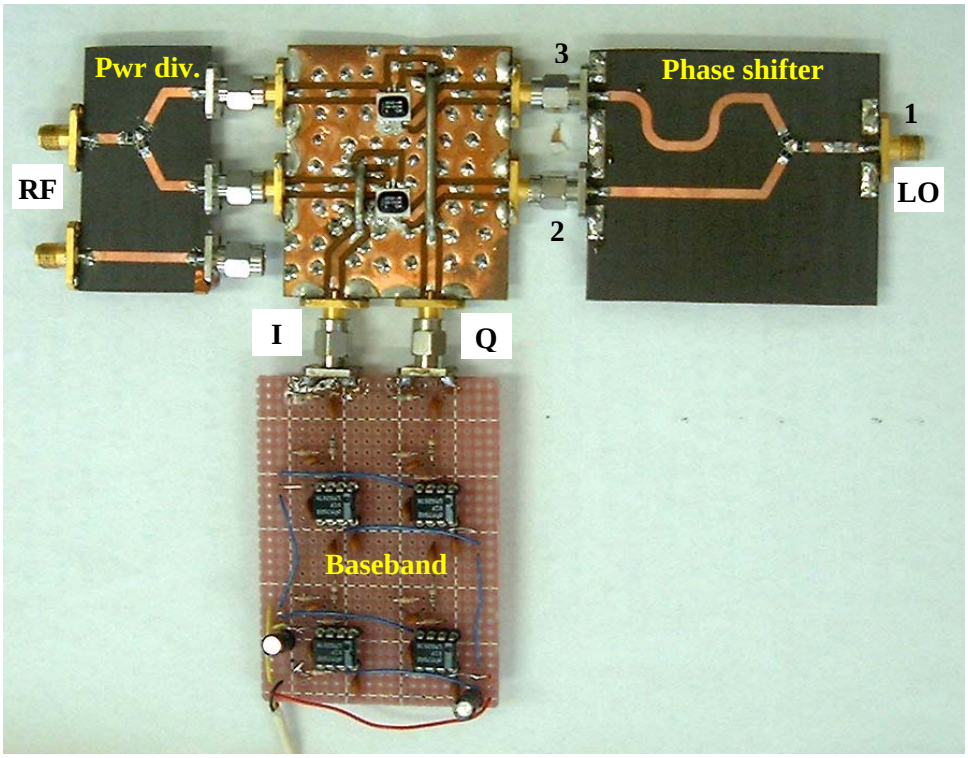


Fig 4.5 Fabrication of the circuit

For measurement and evaluation, the single frequency RF signal is used and its frequency is 1 MHz higher than frequency of LO signal. Therefore, the frequency of baseband signal is 1 MHz. The baseband signals at the output of baseband amplifier are measured and converted to digital signal by using digital oscilloscope. These digital signals of I and Q channel are processed by using DSP algorithm on personal computer (PC).

Fig. 4.6, 4.7 and 4.8 show the simulation and measurement results of phase shifter characteristics. Fig. 4.7 and 4.7 show amplitude ratio and phase difference between port 2 and port 3, respectively. It is shown that the measurement and simulation results have good

agreement. The amplitude difference is below 10%, except 5.4 GHz point, and phase difference depend on the frequency. In the ideal case, phase difference is 90 degree at the frequency of 3.8 GHz, phase imbalance coefficient $\phi$ is zero. Fig 4.8 shows measurement and simulation return loss at 3 ports of phase shifter. It is shown that the return losses are below -15 dB on the frequency range of 1.6-6.0 GHz.

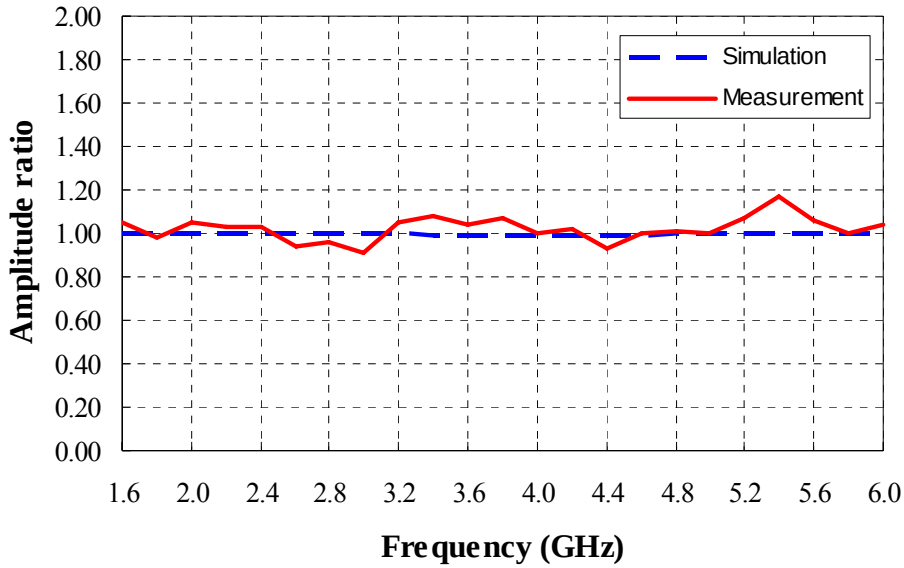


Fig. 4.6 Amplitude ratio at port 2 and 3 of phase shifter

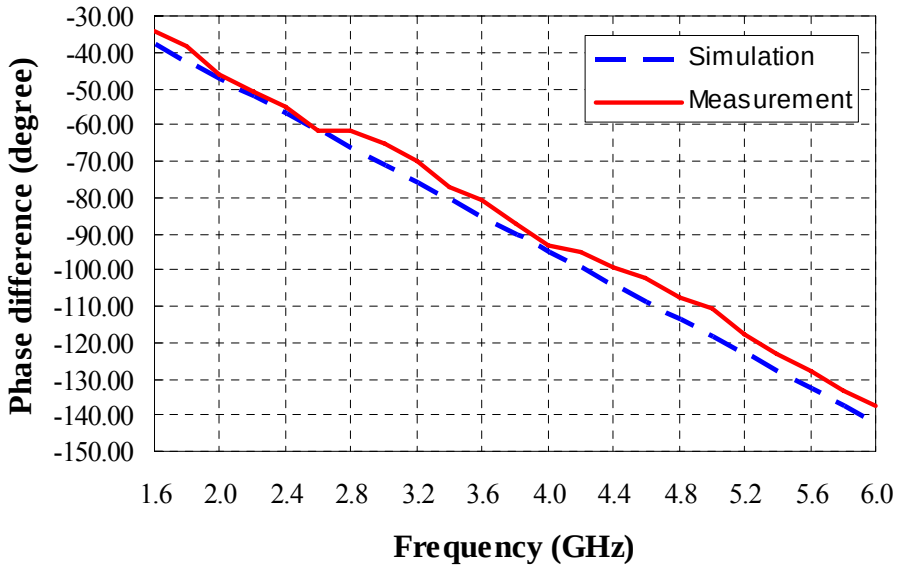


Fig 4.7 Phase difference between port 2 and 3 of phase shifter

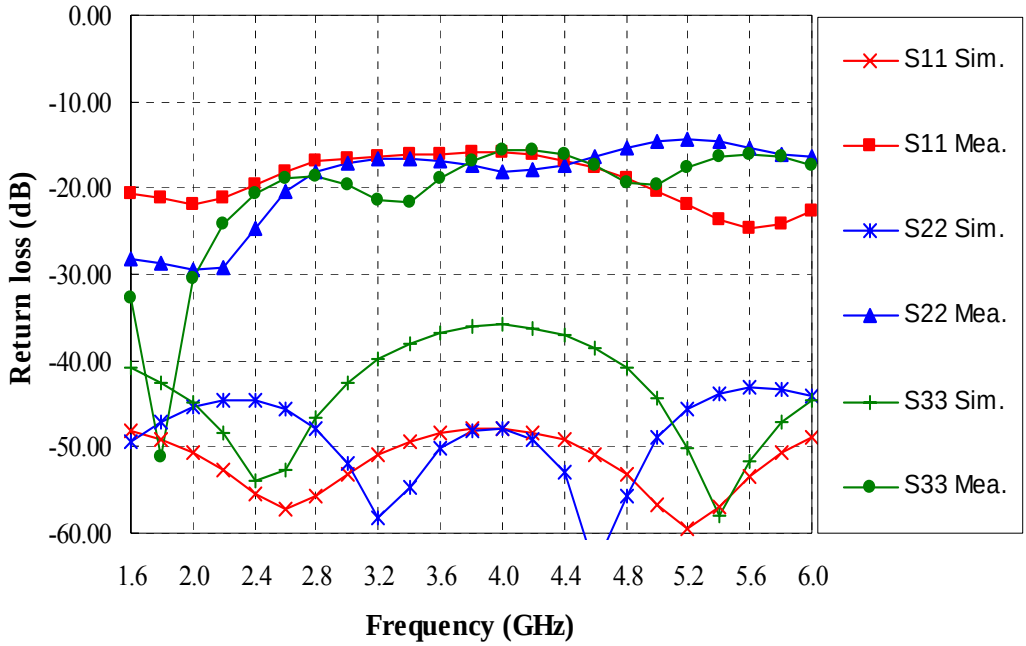


Fig 4.8 Return loss at 3 ports of phase shifter

Fig 4.9 and 4.10 show simulation and measurement results of amplitude and phase imbalance coefficients at the outputs of the baseband amplifier, respectively. The simulation and measurement results have good agreement. From these coefficients, it is show that the band width of the receiver without DSP unit is 0.4 GHz, from 3.6 to 4.0 GHz, because in this frequency range, phase and amplitude imbalance coefficient is below 5 degree and 5%, respectively.

With the application of DSP algorithm, higher imbalance coefficients can be used. Fig 4.11, 4.12 and 4.13 show the Lissajuos graph of the measured, processed and reference I and Q signals at 1.8 GHz, 4.0 GHz and 5.6 GHz, respectively. The Lissajuos graph of reference signal is a perfect circle line with I and Q signals are sin(ωt) and cos(ωt), respectively. The measured signals are the signals at the output of A/D blocks in fig. 4.3. The processed signals are the signals at the output of DSP block in Fig 4.3 with the imbalance coefficient in Fig 4.9 and 4.10. From Fig 4.9 and 4.10, the imbalance coefficients at 1.8 GHz, 4.0 GHz and 5.6 GHz are 0.90, 1.10, and 1.10, respectively for amplitude, and -75.7, 12.1 and 44.5, respectively for phase.

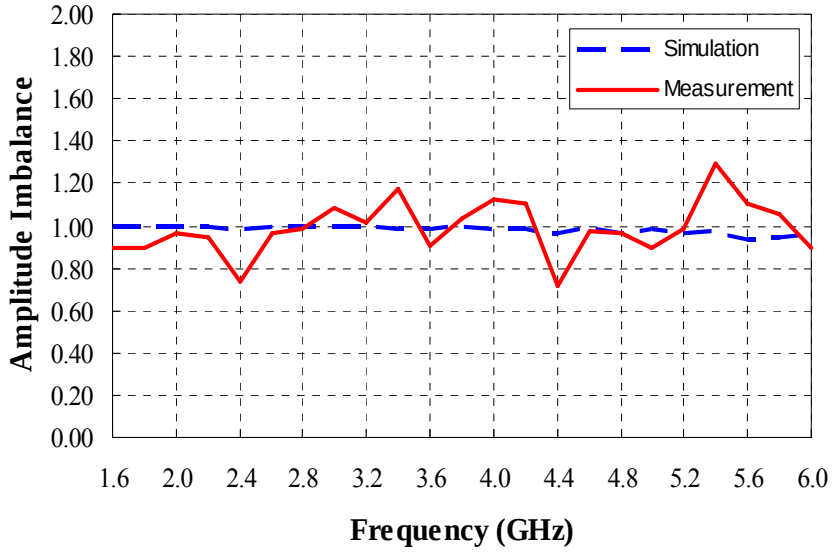


Fig 4.9 Amplitude imbalance coefficient of quadrature down converter

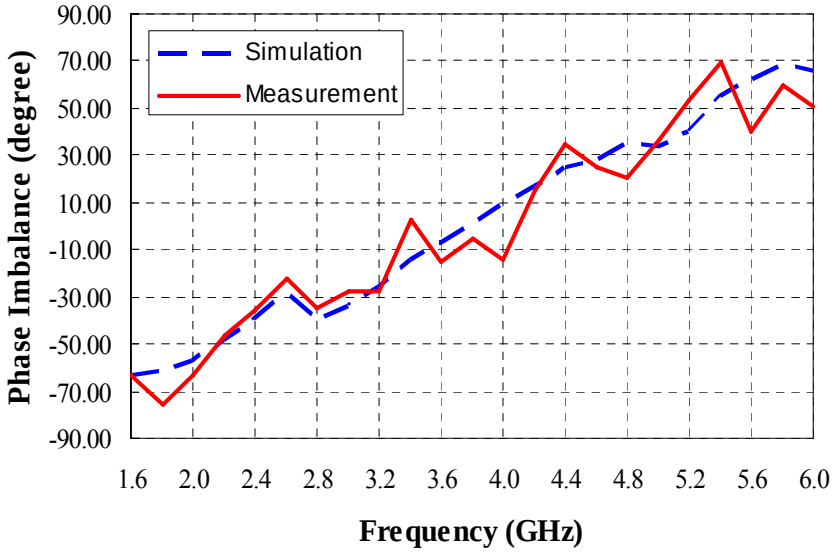


Fig 4.10 Phase imbalance coefficient of quadrature down converter

The measured signals at 1.8 GHz and 5.6 GHz show high imbalance coefficients because the elliptical graphs are narrow. Imbalance coefficients of the measured signal at 4.0GHz are lower than imbalance coefficients at 1.8 GHz and 5.6 GHz.

The processed signals in 3 cases are good agreement with the reference signal. It means that the processed I and Q signals are sin(ωt) and cos(ωt), respectively.

These results show that the quadrature down converter with high imbalance coefficients can be realized with the application of the proposed DSP algorithm. The bandwidth of the receiver can be extended from 0.4 GHz (3.6-4 GHz band) to 4 GHz (1.8-5.8 GHz band) with phase imbalance coefficient in the range of -75 degree – +70 degree and amplitude imbalance coefficient in the range of 0.8 – 1.18.

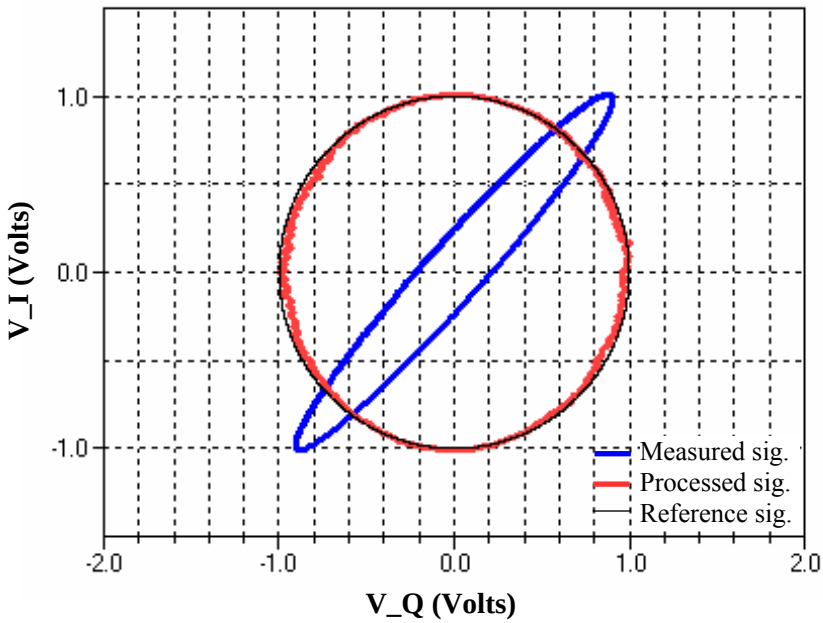


Fig 4.11 Lissajuos graph of the I and Q signal at 1.8 GHz

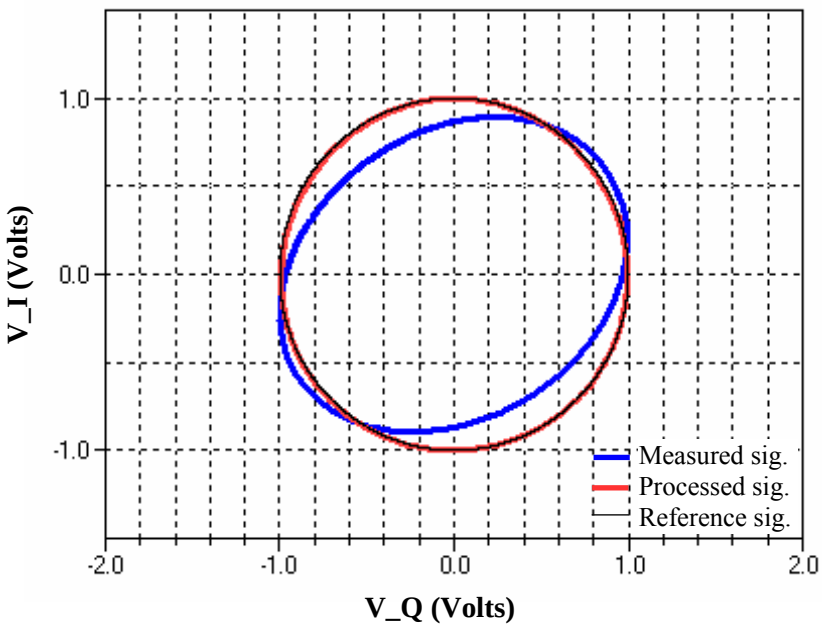


Fig 4.12 Lissajuos graph of the I and Q signal at 4.0 GHz

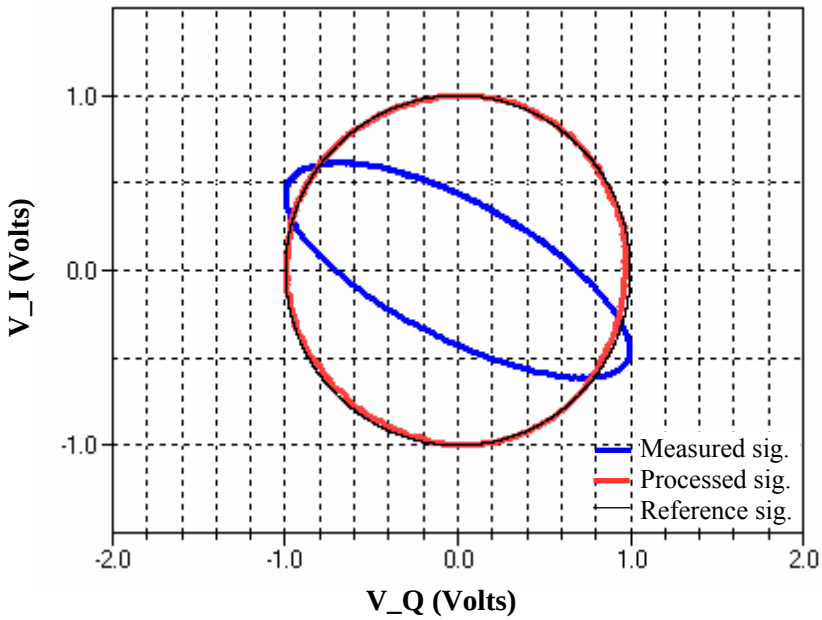


Fig 4.13 Lissajuos graph of the I and Q signal at 5.6 GHz

The method for extending the bandwidth of direct down-conversion receivers is presented in this section. It is the combination of the baseband DSP algorithm and analog front-end circuits. In [19], the authors try to design a wideband 90° phase shifter to cover the frequency range of 0.9-2.5 GHz with low phase ripple. But section 4.2.2 shows that the phase shifter with high phase ripple can be used in quadrature down-converter because the phase error can be compensated by baseband DSP algorithm; section 4 shows the simulation, fabrication and measurement results of the direct down conversion receiver with the simple phase shifter. It is shown that the bandwidth can be extended from 0.4 GHz (3.6-4 GHz band) to 4 GHz (1.8-5.8 GHz band). From these analysis and simulation results, it can be concluded that with the couple of analog front-end circuit and the baseband DSP algorithm, the bandwidth can be extended by using higher ripple phase shifter, analog front circuit becomes simpler, cheaper and more compact.

## 4.3. Design of analog TX circuit

This section presents the design of analog TX circuit for MIMO testbed. As stated before, for circuit simplification and multimode operation, direct conversion techniques are

applied in design of analog TX circuit. This circuit is coupled with the baseband digital signal processing unit to compensate the imbalance characteristics of analog circuit.

### 4.3.1. Transmitter architecture and signal analysis

Fig. 4.14 shows the architecture of the direct up conversion transmitter. In this figure, $g$ and $\phi$ are amplitude and phase imbalance coefficients, respectively, of the circuit. The ideal case is the case of $g = 1$ and $\phi = 0$. In the case of imbalance, two baseband signals $x_I(t)$ and $x_Q(t)$ are controlled to eliminate the effect of imbalance.

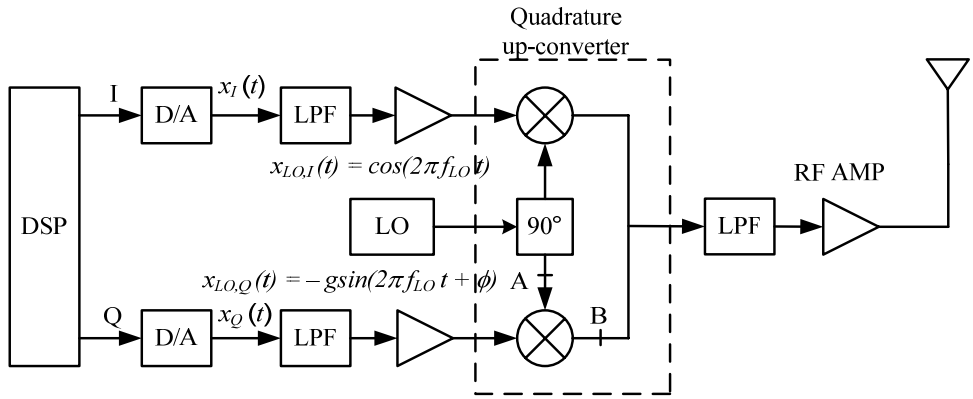


Fig. 4.14 Transmitter architecture and signals in direct up-conversion transmitter

The output of quadrature up-converter is described as (4.9)

$$x_{RF}(t) = x_I(t)\cos(2\pi f_{LO} t) - g x_Q(t)\sin(2\pi f_{LO} t + \phi) \tag{4.9}$$

where $x_I(t)$ and $x_Q(t)$ are the output of I and Q channel of DSP unit. $x_I(t)$ and $x_Q(t)$ can be expressed as (4.10) and (4.11).

$$x_I(t) = \cos(2\pi f_0 t) \tag{4.10}$$

$$x_Q(t) = -g'\sin(2\pi f_0 t + \phi') \tag{4.11}$$

Replace (4.10), (4.11) into (4.9), $x_{RF}(t)$ becomes (4.12).

$$\begin{aligned} x_{RF}(t) = {} & \frac{1}{2}\{\cos[2\pi(f_{LO} - f_0)t] + \cos[2\pi(f_{LO} + f_0)t]\} + \\ & \frac{1}{2} gg'\{\cos[2\pi(f_{LO} - f_0)t + (\phi - \phi')] - \cos[2\pi(f_{LO} + f_0)t + (\phi + \phi')]\} \end{aligned} \tag{4.12}$$

From (4.12), if $g'$ and $\phi'$ are chosen so that $gg' = -1$ and $\phi - \phi' = 0$, $x_{RF}(t)$ becomes (4.13).

$$\begin{aligned} x_{RF}(t) &= \frac{1}{2}\{\cos[2\pi(f_{LO}+f_0)t] + \cos[2\pi(f_{LO}+f_0)t + (\phi+\phi')]\} \\ &= \cos\left[\frac{1}{2}(\phi+\phi')\right]\cos\left[2\pi(f_{LO}+f_0)t + \frac{1}{2}(\phi+\phi')\right] \end{aligned} \tag{4.13}$$

Fig. 4.15 shows spectrum of signal at the output of quadrature up-converter in two cases, before and after imbalance compensation. When $g$ and $\phi$ are measured, the $x_I(t)$ and $x_Q(t)$ are generated with suitable $g'$ and $\phi'$ and the sideband leakage is removed. In fig. 4.15, there is carrier leakage of the mixer, around -30 dB to -40 dB. The carrier leakage can be removed by controlling the dc offset in the mixer, as shown in [26].

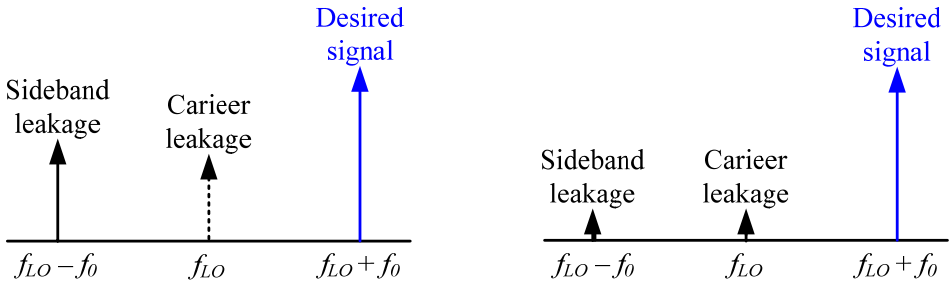


(a) Before compensation (b) After compensation

Fig. 4.15. Spectrum of signal at the output of quadrature up-converter

### 4.3.2. Fabrication and Measurement Results.

Fig. 4.16 and 4.17 show the fabricated circuit of direct up conversion transmitter and measurement setup, respectively. The power combiner and phase shifter circuits are same as the circuits of direct down conversion receiver in section 4.2. The measurement equipments are 2-channel signal generator and spectrum analyzer. The outputs of signal generator are connected to I and Q inputs of the circuit. The RF output is connected to spectrum analyzer. Phase and amplitude of I and Q signals are controlled to minimize the sideband leakage. These phase and amplitude of I and Q signals are shown in fig. 4.18 and 4.19, respectively. These imbalance values will be used in the DSP algorithm. The DC

value of I and Q signals is controlled to minimize the carrier leakage. In this measurement, the frequency of I and Q signal is 1 MHz. Fig. 4.20 and 4.21 show the spectrum of output signal before and after compensation, respectively, at 3.0 GHz.

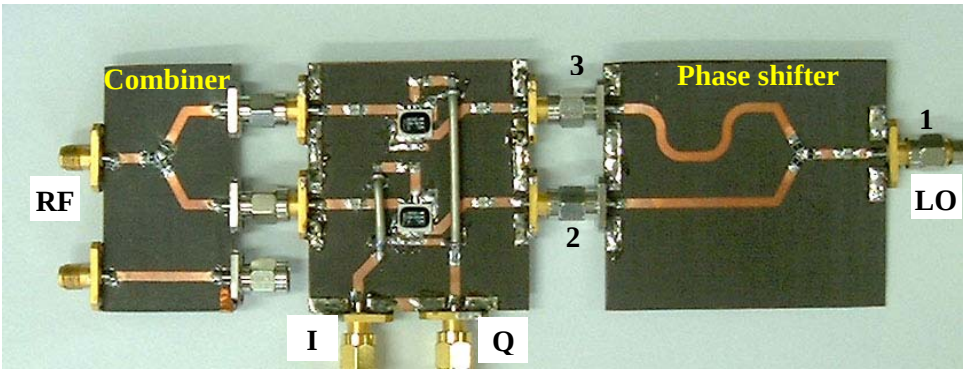


Fig. 4.16 Fabrication of the circuit

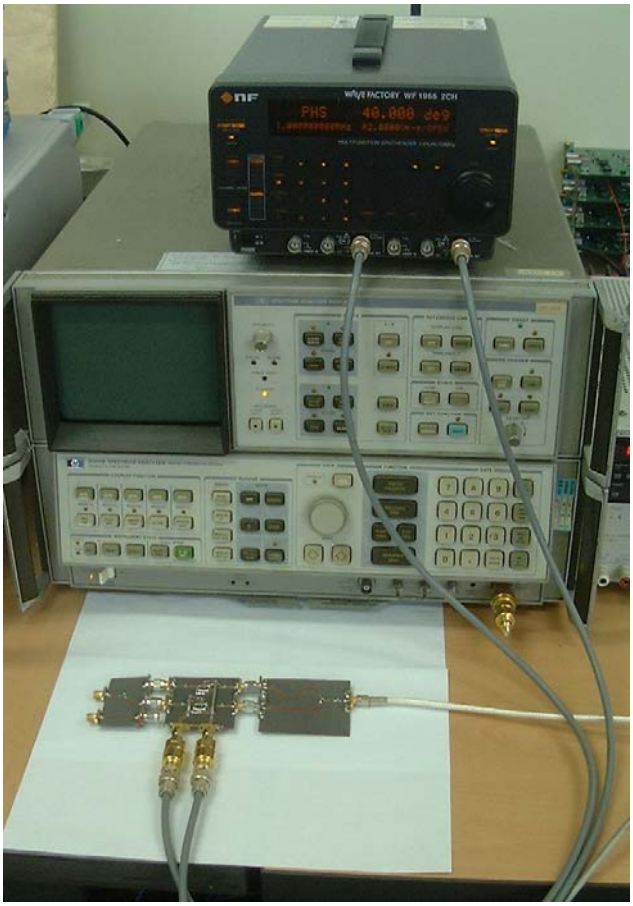

Fig. 4.17. Measurement setup

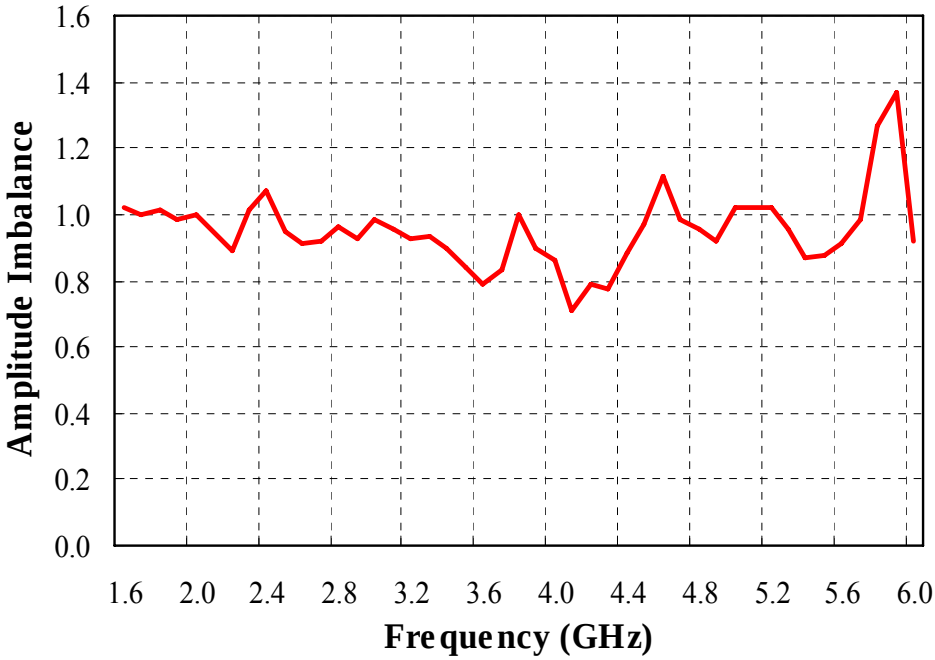


Fig. 4.18 Amplitude imbalance coefficient of quadrature up converter

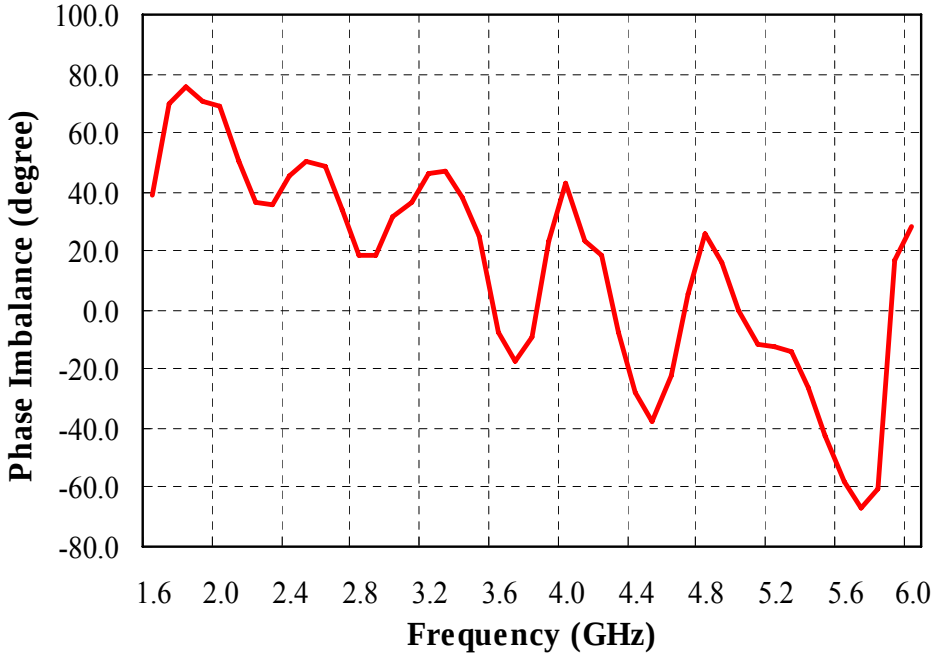


Fig. 4.19 Phase imbalance coefficient of quadrature up converter

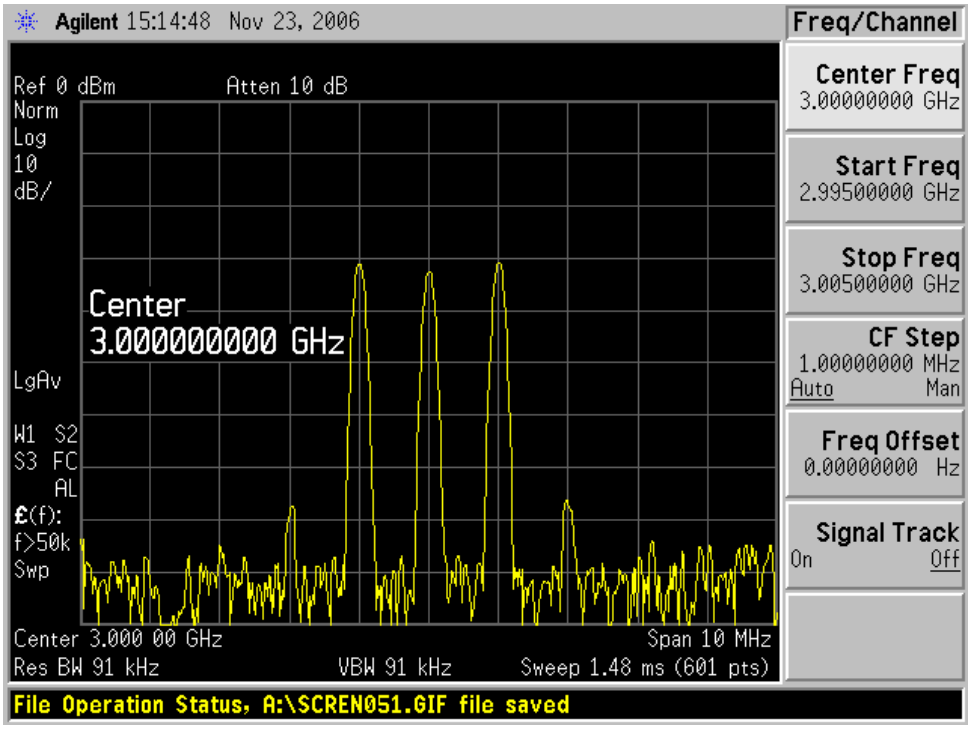


Fig. 4.20 Spectrum of output signal before compensation

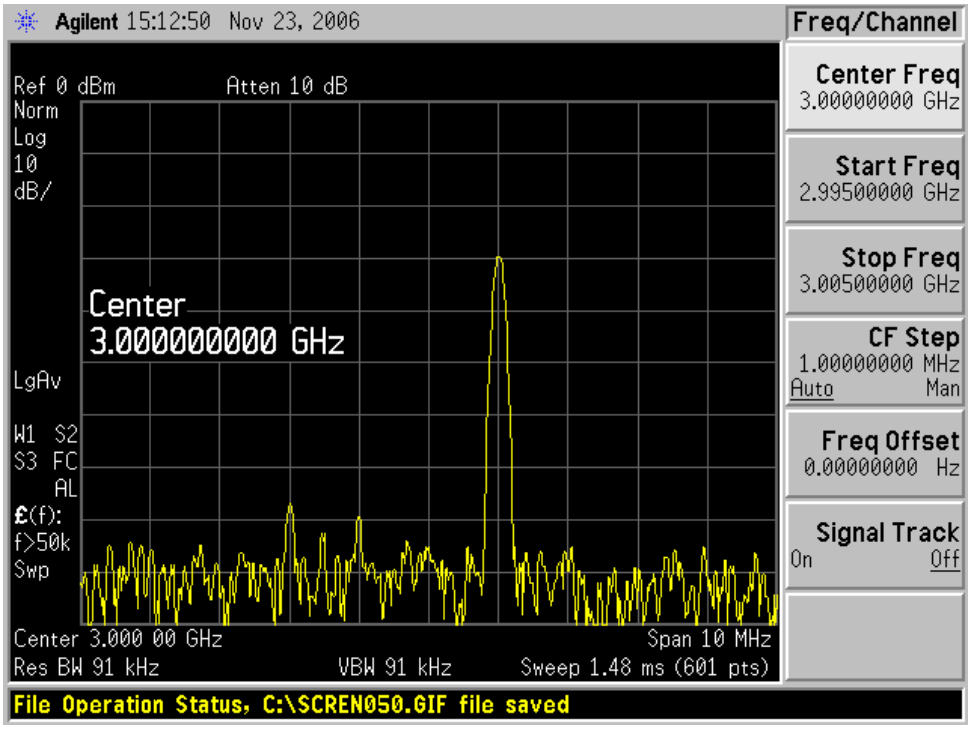


Fig. 4.21 Spectrum of output signal after compensation

## 4.4. Design of 2×2 MIMO measurement system

This section presents the design of MIMO testbed as shown in fig. 4.1. The design consists of hardware and software architecture. In this design, the baseband digital signal processing units are AD, DA systems from Brains Corporation and personal computer (PC).

### 4.4.1 Hardware configuration

Fig. 4.20 shows AD (or DA) system from Brains Corporation. Its specifications are shown in table 4.1. Fig. 4.21 shows the inside configuration of AD, DA systems and the configuration of the designed MIMO testbed. For 2×2 MIMO testbed, 2 direct-up converter and 2 direct down converter are needed; 4 channels of DA and AD systems are used. The AD and DA system are connected to PC via TCP/IP network. The PC is used to develop software, store measurement data and co-operate with AD, DA system for executing signal processing algorithm.

### 4.4.2 Software configuration

Fig. 4.22 shows software components in the MIMO testbed. There are 3 components: software for Windows PC, for SH4/NetBSD and for FPGAs.

The software on PC is developed to perform user interface, AD/DA interface and signal processing tasks. In the first stage of MIMO testbed design, the measurement signals are processed offline. Fig. 4.23 shows the signal processing software for compensating I/Q imbalance in the receiver circuits.

The software on SH-4 CPU is developed to perform the interface between ADC/DAC boards and PC and signal processing tasks.

The FPGA code is used to configure the operation of ADC/DAC boards and perform some real time signal processing tasks.

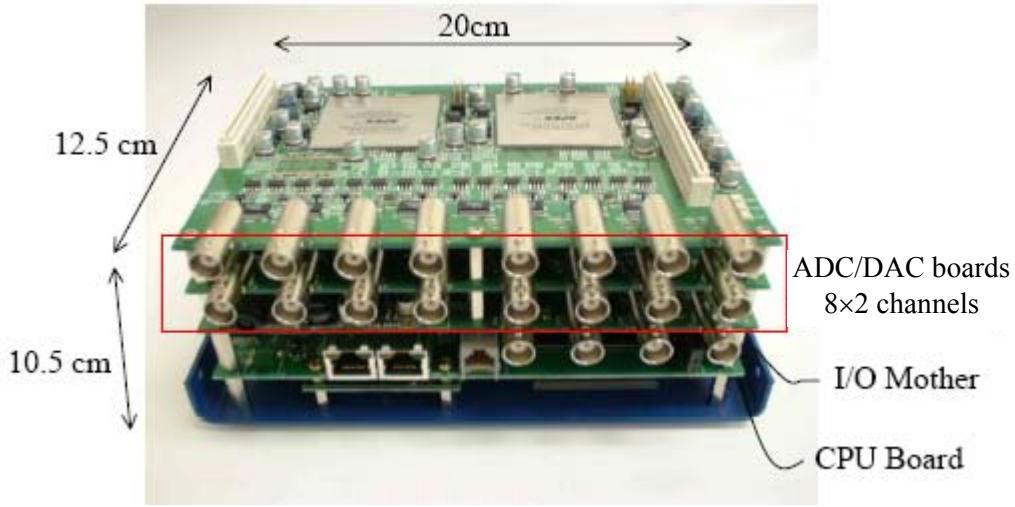


Fig. 4.22 AD, DA system from Brains Corporation

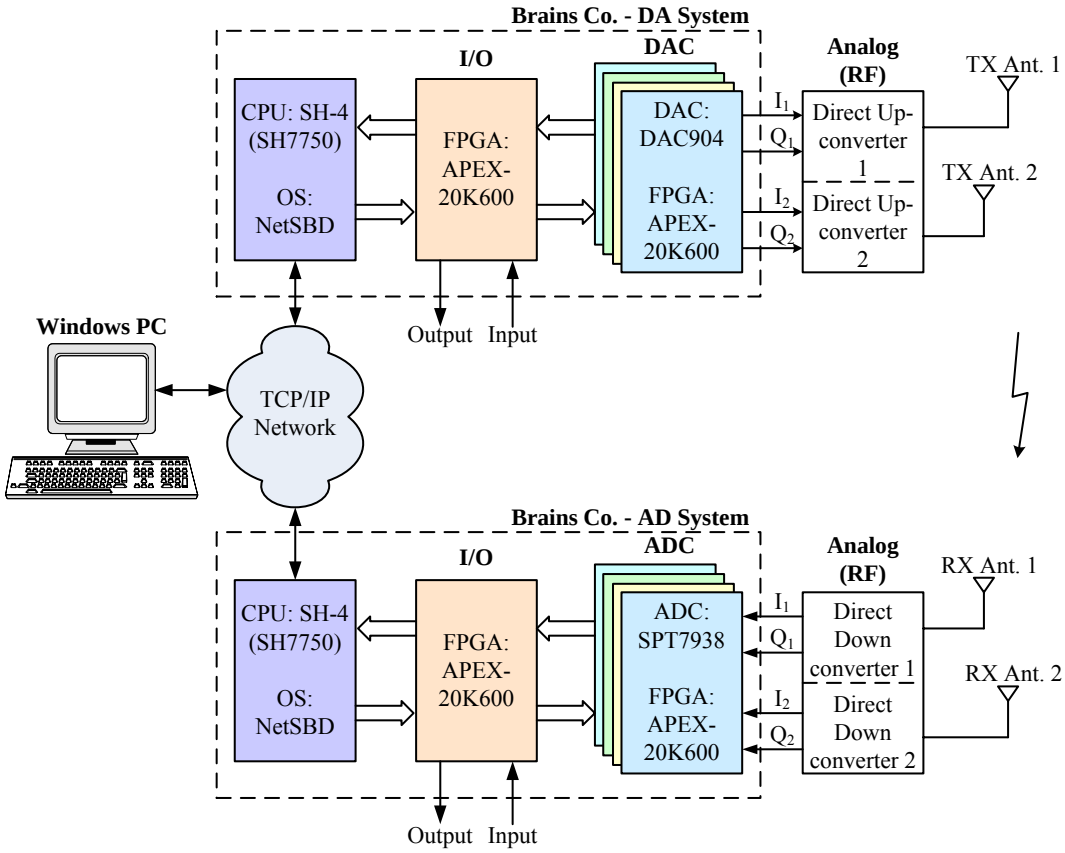


Fig. 4.23 Configuration of MIMO testbed

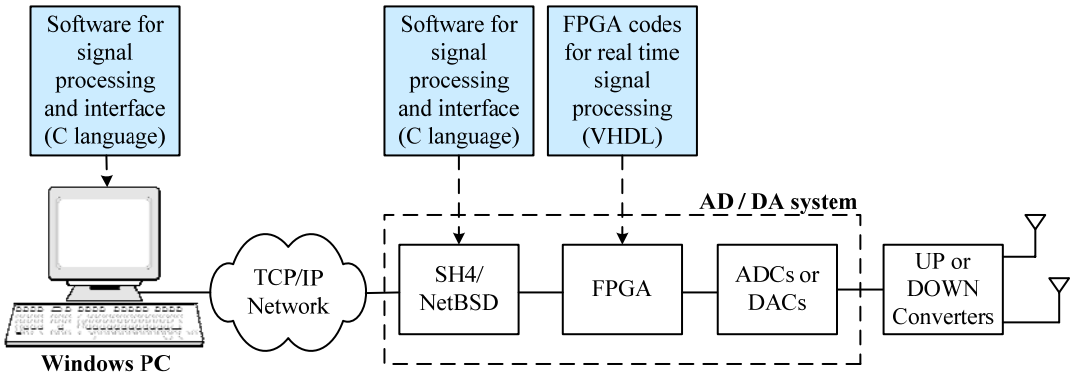


Fig. 4.24 Software components

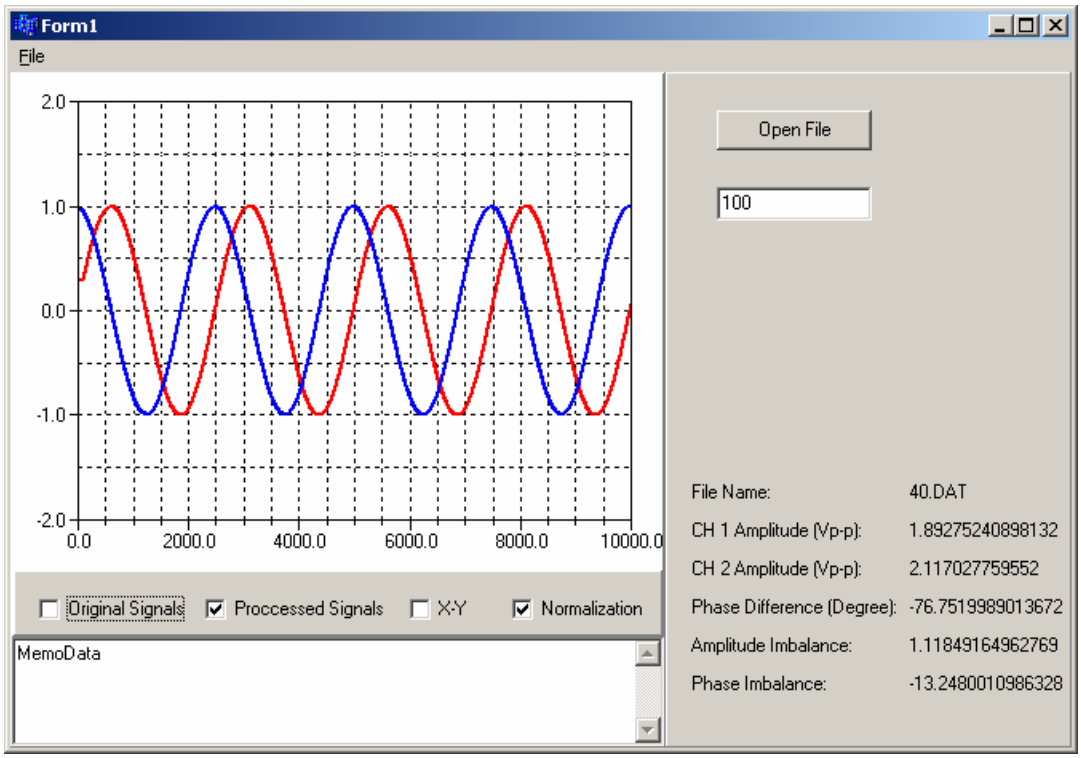


Fig. 4.25 Software for I/Q imbalance compensation

## 4.5. Summary

To develop a MIMO testbed, Agilent Advance Design System (ADS) software is used to simulate the RF analog circuits, AD/DA systems from Brains Corporation and personal computer (PC) are used as the baseband DSP hardware of testbed. These circuits are fabricated and its parameters are measured and shown in this thesis. Some DSP functions

are developed and also shown in this thesis. As shown in [3], the development of MIMO testbed require long time because it relates to many study fields such as coding, synchronization, the operation and optimal programming of baseband processors, the impact of radio frequency (RF) imperfections on signals, the operation of test equipment, and deployment in realistic test scenarios. Therefore, in this thesis, the testbed design is not complete; some works remains for further study.

# CHAPTER 5

# CONCLUSION

The improvement of algorithm for antenna measurement software and development of measurement testbed for multi-input multi-output (MIMO) antenna measurement are presented. In chapter 2, the structure of the antenna measurement software is improved. With this structure, the software can be operated on variety types of equipment, can be modified easily and can measure 4 parameters with noise reduction function. Four parameters are antenna gain, 2-D radiation pattern, 3-D radiation pattern and polarization. In addition, the filter algorithm is developed for reducing measurement noise. With the application of the filter algorithm, the measurement time and error are improved. In chapter 3, MIMO antenna characteristics such as gain diversity, polarization diversity and mutual coupling are measured and calculated on practical measurement system with a sample of EUT. The results show that EUT has good pattern diversity and low pattern correlation coefficients. These results of measurement and evaluations are useful for MIMO antenna designer in improvement of antenna characteristics. In chapter 4, the design of MIMO testbed is presented with fabricated analog front end circuits and testbed configuration. It can be concluded that with the couple of analog front-end circuit and the baseband DSP algorithm, analog front end circuit becomes simpler, cheaper and more compact. Finally, hardware and software configurations of 2x2 MIMO testbed are designed and presented. This MIMO testbed will be used to measure and evaluate other parameters of MIMO antennas such as antenna type, spacing, configuration, number of elements. This study will be done in the future.

# References


[1] Young-Hwan Park, “A study on construction of antenna measurement environment,” Master Thesis, Korea Maritime University, Feb. 2005

[2] Mythri Hunukumbure, *"The MIMO channel: Measurements and Modeling,"* Next Generation Wireless Net Workshop, , Edinburgh, UK, 15 - 17 June 2005.

[3] R. Rao, W. Zhu, S. Lang, C. Oberli, D. Browne, J. Bhatia, JF Frigon, J. Wang, P. Gupta, H. Lee, D.N. Liu, S.G. Wong, M. Fitz, B. Daneshrad,O. Takeshita, *“Mulit-Antenna Testbeds for Research and Education in Wireless Communications,”* IEEE Communications Magazine, December 2004.

[4] Hewllet Packard, HP8530A MICROWAVE RECEIVER USER’S GUIDE, 3rd edition, Feb. 1994

[5] C.A. Balanis, ANTENNA THEORY – ANALYSIS AND DESIGN, 2nd edition, John Wiley & Sons Inc., 1997.

[6] Simon Haykin, AN INTRODUCION TO ANALOG & DIGITAL COMMUNICATIONS, John Wiley & Son, Inc., 1989

[7] Alberto Leon-Garcia, PROBABILITY AND RANDOM PROCESSES FOR ELECTRICAL ENGINEERING, 2nd edition, Addison-Wesley Publishing Company, Inc., 1994

[8] Robert M. Gray, Lee D. Davisson, AN INTRODUCTION TO STATISTICAL SIGNAL PROCESSING, Cambridge University Press, 2004

[9] K. S. Min, T. N. Tran, C. K. Park, *“Combination of space and time adaptive mean filters for noise reduction in antenna measurement,”* Proceeding of 2005 Asia-Pacific Microwave Conference, December 2005

[10] TOYO Corp., TY2100AO – OUTPUT ANALYSIS SOFTWARE, Ver. 1.15, July 2005

[11]Kati Sulonen, Pasi Suvikunnas, Lasse Vuokko, Jarmo Kivinen, and Pertti Vainikainen, *“Comparison of MIMO Antenna Configurations in Picocell and Microcell Environments,”* IEEE Journal on selected areas in communications, VOL. 21, NO. 5, pp. 702-712, June 2003

[12] York EMC Services Ltd, University of Bristol, University of York, BT Exact Technologies, Toshiba Research Europe Limited, PROJECT REPORT: ANTENNA DESIGN FOR MIMO SYSTEMS, 2003-2004

[13] K. S. Min, T. N. Tran, *"An enhanced antenna measurement program in anechoic chamber,"* Proceeding of the Korean Society of Marine Engineering 2005 first conference, pp. 369-374, June 2005

[14] Ian Glover, Peter Grant, DIGITAL COMMUNICATIONS, Prentice Hall, pp. 110, 1998

[15] Kati Sulonen, Pertti Vainikainen, *"Performance of mobile phone antennas including effect of environment using two methods,"* IEEE transactions on instrumentation and measurement, vol. 52, no. 6, pp. 1859-1864, December 2003

[16] Mythri Hunukumbure, *"The MIMO channel: Measurements and Modeling,"* Next Generation Wireless Net Workshop, , Edinburgh, UK, 15 - 17 June 2005

[17] Asad A. Abidi, *"Diret-conversion radio transceiver for digital communications,"* IEEE Journal Of Solid-State Circuits, Vol 30, No 12, pp. 1399-1410, December 1995

[18] S. Mirabbasi and K. Martin, *"Classical and modern receiver architecture,"* IEEE Commun. Mag., vol. 38, pp. 132-139, Nov.2000

[19] Tadao Nakagawa, Munenari Kawashima, Hitoshi Hayashi, and Katsuhiko Araki, *"A 0.9-2.5 GHz wideband direct conversion receiver for multi-band applications,"* IEEE - GaAs IC Symposium, 23rd Annual Technical Digest, pp. 37-40 2001

[20] Schiffman, B.M., *"A New Class of Broad-Band Microwave 90-Degree Phase Shifters,"* IRE transactions on microwave theory and techniques, pp. 232-237, April 1958

[21] JosC Luis Ramos Quirarte, and J. Piotr Starski, *"Novel Schiffman phase shifters,"* IEEE transactions on microwave theory and techniques, vol. 41, no. 1, pp. 9-14, January 1993.

[22] Yong-Xin Guo, Zhen-Yu Zhang, and Ling Chuen Ong, *"Improved wide-band Schiffman phase shifter,"* IEEE transactions on microwave theory and techniques, Vol. 54, No. 3, pp. 1196-1200, March 2006

[23] Sanjit K. Mitra, DIGITAL SIGNAL PROCESSING – A COPMUTER BASED APPROACH, 2nd Edition, Mc Graw Hill, pp. 603, 2002

[24] Paul Burns, SOFTWARE DEFINED RADIO FOR 3G, Artech House, pp. 56, 2002

[25] Heinrich Meyr, Marc Moeneclaey, Stefan A. Fechtel, DIGITAL COMMUNICATION RECEIVERS – SYNCHRO-NIZATION, CHANNEL ESTIMATION,AND SIGNAL PROCESSING, John Wiley & Sons, Inc, pp. 219, 1998

[26] N. Vasudev and Oliver M. Collins, Fellow, IEEE, *"Near-Ideal RF Up-converters,"* IEEE transactions on microwave theory and techniques, Vol. 50, No. 11, pp. 2569-2575, November 2002